THERMOPLASTIC COATING OF CARBON FIBERS

Final Report

by

D. D. Edie and G. C. Lickfield
Center for Advanced Engineering Fibers
Clemson University
Clemson, SC 29634-0909

sponsored by

the National Aeronautics and Space Administration
Langley Research Center
Hampton, VA 23665

NASA Research Grant NAG-1-680

Robert M. Baucom
NASA Technical Officer

THERMOPLASTIC COATING OF CARBON FIBERS

Final Report

by

D. D. Edie and G. C. Lickfield
Center for Advanced Engineering Fibers
Clemson University
Clemson, SC 29634-0909

sponsored by

the National Aeronautics and Space Administration
Langley Research Center
Hampton, VA 23665

NASA Research Grant NAG-1-680

Robert M. Baucom
NASA Technical Officer

ABSTRACT

Thermoplastic polymers are under extensive evaluation for use as matrix materials for composites. The major obstacle to the use of these promising polymers is that their high viscosity makes liquid impregnation of the carbon fiber tows difficult. One alternative is to coat the fibers with the thermoplastic in a dry, finely-ground powder form.

Using a continuous powder coating process, more than 1500 meters of T 300/LaRC-TPI prepreg were produced for the current study. Two different types of heating sections in the coating line, namely electrical resistance and convection heating, were utilized. These prepregs were used to fabricate unidirectional composites. During composite fabrication the cure time of the consolidation was varied, and composites samples were produced with and without vacuum.

Using these specimens, the effects of the different heating sections and of the variation of the consolidation parameters on mechanical properties and void content were investigated. The void fractions of the various composites were determined from density measurement, and the Mechanical properties were measured by tensile testing, short beam shear testing and dynamic mechanical analysis.

The results of this investigation showed that composites formed using LaRC-TPI powder-coated prepreg contained very few voids when heated rapidly during consolidation. Only moderate tensile strengths were obtained, but short beam shear test and dynamic mechanical analysis indicated a good interfacial bonding between the matrix and the carbon fibers.

ACKNOWLEDGEMENTS

This study was supported by the Langley Research Center of the National Aeronautics and Space Administration under grant number NAG 1-680. Mr. Robert M. Baucom served as Langley Research Center's technical officer for the project.

TABLE OF CONTENTS

Table of Contents (Continued)

LIST OF TABLES

LIST OF FIGURES

List of Tables (Continued)

CHAPTER 1

INTRODUCTION

For high performance applications, the high specific strength and stiffness of composites often make them preferable to conventional materials, such as steel or aluminum. Because of their low cost, thermosets are the most widely used matrix material for polymeric composites. However, their limited toughness and repairability have led to the development of thermoplastic matrix polymers. Many of these new, recently developed, thermoplastic polymers exhibit superior physical and thermal properties when used in carbon fiber composites. However, their high viscosity and low solubility make conventional hot melt and solution prepregging methods extremely difficult. A new method to coat continuous fibers with thermoplastic polymer, a dry powder coating process, was developed at Clemson University by Gantt [1] and Allen [2] in a NASA sponsored project. After the tow has been spread using a pneumatic device, the process utilizes a fluidized bed to apply the thermoplastic powder to the tow. Finally, the coated tow is heated, melting the polymer onto the individual fibers. Using this process, a fiber bundle with a flexibility approaching that of uncoated fiber can be obtained.

In this work, the continuous powder coating system was used to coat carbon fibers with LaRC-TPI, a thermoplastic polyimide invented at the Langley Research Center of NASA. The prepregs were formed into unidirectional composites, whose mechanical properties were determined with tensile tests, short beam shear tests and dynamic mechanical analysis. The results of this evaluation are detailed and discussed in the following chapters.

CHAPTER 2

LITERATURE REVIEW

2.1 Composites

Fiber reinforced composite materials consist of fibers of high strength and modulus embedded in a matrix. Although both the fibers and the matrix retain their individual properties and chemical identities, a composite of these materials exhibits properties that can not be achieved with either of the constituents alone [3].

Unlike conventional materials like steel or aluminum, which exhibit directionally-independent behavior, composites are often anisotropic materials. Since the fibers are the strongest and stiffest component, a composite is strongest when loaded in the fiber direction. In all other directions of loading, the strength and stiffness are lower. This can be viewed as disadvantage, but a benefit can be derived from this anisotropy. The use of composites materials allows the designer to tailor the material to meet particular structural requirements [4]. Composites can be made strong or weak in every desired direction, depending upon the amount of as well as the alignment of reinforcing fibers. Bi- or multidirectional reinforcement yields a more balanced set of properties. In addition to the strength and stiffness, other properties, such as thermal expansion and thermal conductivity, can be altered in composite structures. Since carbon fibers, unlike most other materials, have a negative thermal expansion coefficient along their length, composites consisting of carbon fibers and a polymer matrix can be designed to produce a coefficient of thermal expansion close to zero. This dimensional stability over a wide range of temperature makes carbon fiber-reinforced composites attractive for aerospace applications, such as support structures for mirrors and lenses [5]. Thermal expansion in space mirrors is particularly critical since small changes in temperature can impair their accuracy.

Besides these structural differences, their light weight gives composites additional advantages. The low density of composite materials, combined with their excellent strength and stiffness, makes their strength-to-weight ratio as well as the modulus- weight ratio considerably higher than those of metals. Thus, as Figure 1 [6] shows, the specific tensile strength, specific modulus, as well as other properties of composites, are superior to most conventional materials. An additional advantage of composites is their greater toughness and resistance to crack propagation. This is caused by fiber pull-out and matrix deformation during fracture. The sliding friction between the fibers and the matrix during the pull-out of fibers results in load-transfer, a toughening mechanism, during fracture. Also, if the fiber fails before the matrix, work is done in deforming the matrix itself, an additional toughening mechanism [4]. Composites are usually extremely chemically resistant, however, many polymer matrices of composites are capable of absorbing moisture from the surrounding environment which can deteriorate their properties.

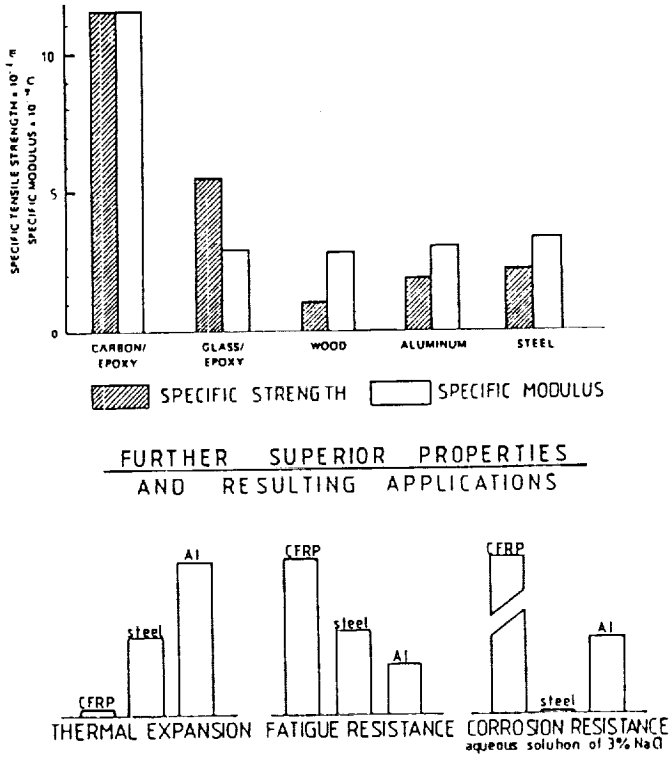

Figure 1. Composites versus conventional materials.

In summary, in many aspects composites are superior to conventional materials. To date, however, their high cost has limited their application. This expense can be attributed to both the cost of raw materials and the complicated production techniques employed. Therefore, one path to lower-cost composites is to improve and simplify the processing. Many of the processing difficulties can be traced to the brittle nature of the fiber and the fluidity of the most common matrix material, polymers.

2.2 Polymeric Matrix

The matrix holds the fibers in the desired alignment, distributes any applied load among the fibers, supports the fibers during compression loading and protects them from environmental moisture and chemical corrosion or oxidation. There is a multitude of materials which can be chosen for the matrix. In addition to the polymeric materials, aluminum and magnesium alloys, as well as ceramics and carbon, can be employed as the matrix, but only polymers shall be discussed in depth.

Polymers are divided into two broad categories: thermoplastics and thermosets. In a thermoplastic polymer, individual molecules are linear or branched in structure with no chemical linkage between them. They are held in position by weak secondary bonds (intermolecular forces), such as van der Waals forces and hydrogen bonds. The strength of these bonds depends on the distance between the molecule chains. If pressure and heat are applied to the specimen, these bonds can be broken, allowing the molecules to move freely among each other. This enables thermoplastics to be remelted; thus, thermoplastics parts can be reshaped as many times as desired. In contrast, in a thermoset polymer chemical bonds join the molecules, forming a three-dimensional structure. This structure is neither fusible nor soluble. These crosslinking bonds are formed during a process called curing, and, once cured, a thermoset polymer can not be melted.

Thermoset matrices dominate the market for matrix materials because of their low cost and fluidity [7]. They can be supplied in a monomeric or oligomeric state, characterized by low viscosity. A low viscosity simplifies the incorporation of fibers into the matrix polymer. Good wetting and impregnation are essential for strong bonding between fiber and matrix. Epoxies are the most widely used matrix material in aerospace and aircraft applications. Using different curing agents, the properties of these epoxies can be optimized. Unsaturated polyesters represent another class of thermosets which commonly are used in automotive, marine, chemical, and electrical applications. Most thermoset polyesters exhibit low glass transition temperatures and lower moduli, but they are also less expensive than epoxies. Another group of thermosets is the phenolics, produced from the polycondensation of phenol and formaldehyde. The water byproduct of the curing reaction creates problems because it can form cracks and voids in the material. However, the excellent flammability resistance and long term thermal stability of phenolics help them to maintain their market position [8].

An especially important group of high performance matrix resins is the polyimide family, which includes both condensation- and addition-type thermosets, as well as thermoplastic resins [5]. The mechanical properties of polyimides are often sustained above 600°F, far beyond the degradation temperature of many other polymers. Polyimide composites are often difficult to fabricate. Frequently, a solution of polyamic acid in a high boiling solvent is painted onto the fiber as a lacquer or varnish to form prepregs, which then may be laid up and cured. A drawback of this process is that, because of the need to drive out solvent and condensation volatiles to avoid void formation, the curing step can be difficult. Polyimides possess outstanding toughness in comparison with other thermosets.

Although the properties of the thermosets can differ tremendously, the exact properties needed for a composite always represent a compromise between the required thermal stability and the toughness. If the number of crosslinks per unit volume is high, mobility of the chains in the matrix polymer is reduced, increasing the mechanical properties and

thermal stability of the composite. Unfortunately, this increase in mechanical properties is coupled with an increase in brittleness. This fact has led to the development of thermoplastics whose toughness and fatigue resistance, which are extremely important in structural applications, are higher than those of thermosets. While typically these materials are not stable at high temperatures, recent developments have improved their high temperature performance. There are six main varieties of thermoplastic materials: polyarylene ethers or sulfides, polysulfones, polyester, amide or amideimide polymers and polyimides [9]. An example of the polyarylene group of polymers is polyetheretherketone, PEEK. Since PEEK has good toughness and excellent processibility, it is currently the thermoplastic of choice. Even though the relatively low glass transition temperature of PEEK (143°C) limits its use in high temperature environments, it displays very low creep up to a temperature of 250°C [10]. Another promising group of thermoplastics is the polyimides, which like thermoset polyimides are known for their thermooxidative stability and solvent resistance.

Their high toughness and high strain-to-failure make thermoplastic polymers more resistant to matrix microcracking in the composite laminate and contribute to their high impact strength. However, there are numerous other advantages of thermoplastics which can be listed as well [3]:

- unlimited storage life at room temperature;
- shorter fabrication time;
- postformability;
- ease of repair by welding or solvent bonding;
- ease of handling (no tack).

There are numerous economic advantages for using thermoplastic matrix materials. If a thermoset composite part is damaged during its production, it is usually worthless. In

contrast, thermoplastic composites often can be remelted and reformed, which is especially desirable when high priced resins and fibers are being used for advanced composites. The tackiness of most thermosets hinders automated production, therefore expensive hand-lay is often required. Since thermoplastics do not need to be cured, fabrication times can be reduced, making mass production possible. Nevertheless, thermoplastics will not readily replace thermosets. The high melt or solution viscosity of the thermoplastics makes it difficult to incorporate continuous fibers into matrix polymer. This problem can be overcome by preparing thermoplastics with lower viscosities or by improving the incorporating process itself. Both approaches, namely the development of a new thermoplastic powder, LaRC-TPI, and a dry coating process to produce a textile preform, are described in the following sections. The goal of both procedures is improved processibility.

2.3 LaRC-TPI

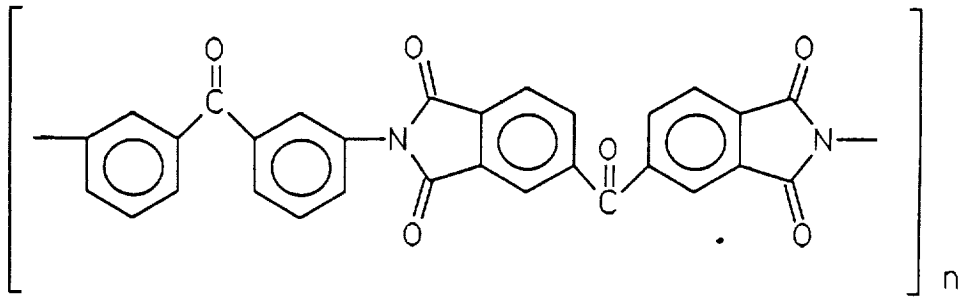

LaRC-TPI

Figure 2. Chemical structure of LaRC-TPI.

LaRC-TPI (Langley Research Center Thermoplastic Polyimide) is a linear aromatic polyimide (Figure 2) developed by NASA in the late 1970's. A precursor to LaRC-TPI had been developed as a structural adhesive for bonding titanium. Since LaRC-TPI

exhibited adequate thermoplastic flow, it could be used to bond large areas without forming voids [11]. However, compared to other thermoplastics, the degree of flow that can be obtained at a given temperature for LaRC-TPI is quite low. With the development of a LaRC-TPI imidized molding powder produced by Mistsui Toatsu of Japan, the melt-flow properties were improved. Initially, upon melting, this version of LaRC-TPI shows a much lower viscosity than previous polyimide materials [11]. However, the melt viscosity is quite time-dependent. Figure 3 shows the magnitude of complex viscosity, determined at a frequency of 10 rad/s, as a function of cure time. Using a rotary rheometer Burks et al. [11] measured the complex viscosity of LaRC-TPI powder, lot number 72-501. At any given cure temperature the viscosity increases with increasing the cure time, but during the initial cure stage it remains low. Burks [11] explained this behavior as a crystalline transformation during melting. He postulated that this crystallinity possessed different melting and glass transition temperatures, depending on cure time and cure temperature (Table 1). If the powder is heated to temperatures above 330° C, the crystallinity of the polymer diminishes until finally the material becomes totally amorphous. This unusual behavior of the LaRC-TPI powder, namely its low initial viscosity, can be utilized in its application as a matrix material.

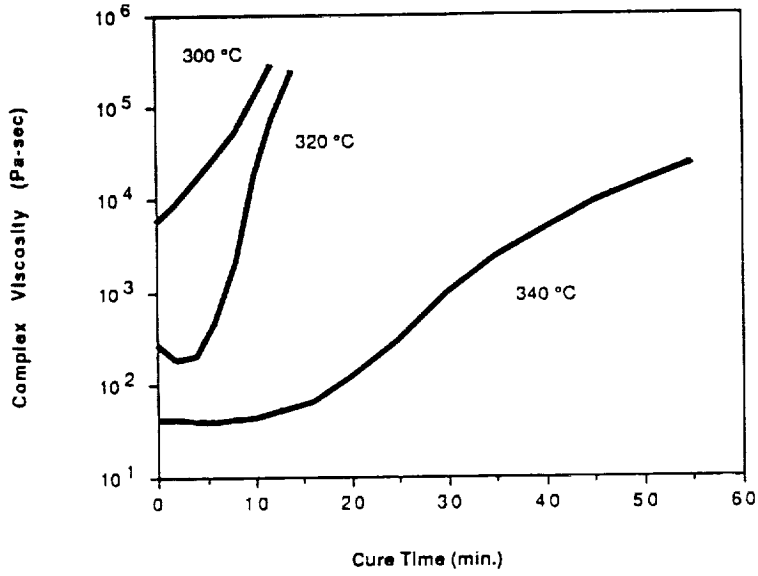

Figure 3. Time dependent viscosity of LaRC-TPI.

Table 1. Dependence of the melt and glass transition temperatures on cure time.

Cure Temperature	Cure Time (minutes)			
	0	15	30	45
°C	Tg (Tm) °C	Tg (Tm) °C	Tg (Tm) °C	Tg (Tm) °C
300	210 (329)	211 (332)	216 (335)	221 (334)
310	215 (330)	221 (337)	227 (339)	231 (340)
320	214 (344)	226 (341)	237 (344)	241 (347)
330	215	232	243	249
340	216	239	244	251

2.4 Dry Polymer Coating

Most commercial prepregs used to form composites are produced by solution/slurry or hot melt impregnation of the fiber tow bundles with matrix polymer [12]. LaRC-TPI, like many of the new generation of thermoplastic matrix polymers, requires new developments in order to solve the variety of problems created by its low degree of solubility and high viscosity. Techniques such as hot melt fusion from matrix films, because of the relatively small melt flow of thermoplastics, provide a marginal polymer penetration in tow bundles and, thus, yield a non-uniform prepreg with poor quality. These problems, coupled with difficulties in solvent removal, can be circumvented by dry polymer coating. In this process small polymer particles are applied to the tow, followed by melt fusion of the particles on individual fibers. Since only neat polymer particles are utilized, no solvent must be extracted after polymer penetration. This prepreg production process consists basically of three steps (Figure 4):

- tow spreading;
- powder coating;
- powder fusion.

Tow spreading plays a very important role because it permits single fibers to be coated. Once spread, the tow is moved through a fluidized bed of powder, where the polymer particles deposit on the fibers. After coating, heat is applied to the fibers and powder so that the melted powder wets the fibers. The result is a flexible pregreg composed of a large number of individually coated fibers.

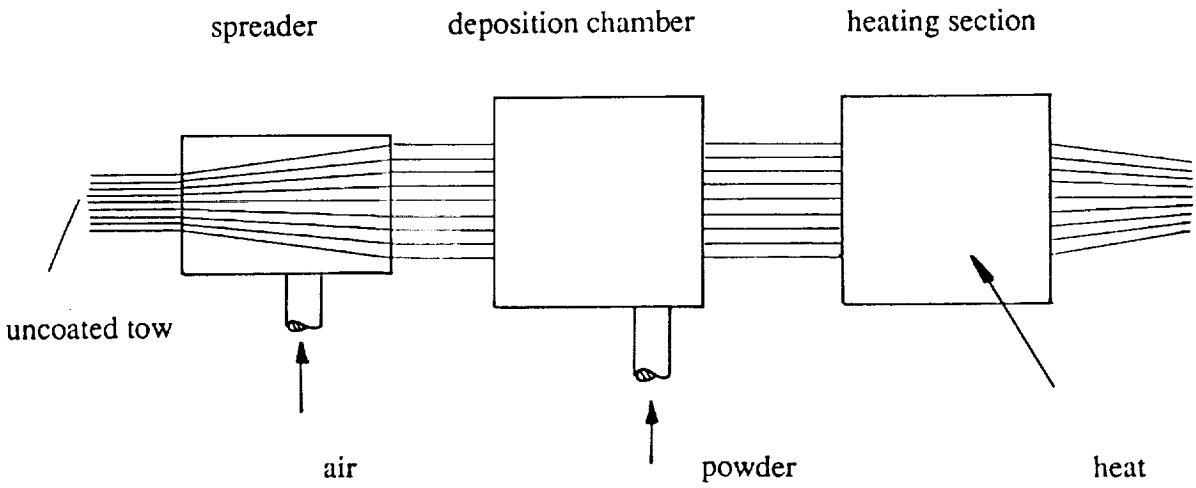

Figure 4. Schematic of dry polymer coating process

Research using the above process is being conducted at several research faculties, namely Georgia Institute of Technology, the University of Akron, Langley Research Center and Clemson University [12]. Each research group is developing a continuous process to produce the dry coated tow. Since the fiber is brittle and tends to break easily, the tow tension must be carefully controlled. Furthermore, for the optimum performance

of the pneumatic spreader used in many of these processes, a constant tension is vital. These pneumatic spreaders apply an air stream perpendicular to the fiber tow alignment to force the tow to spread. The use of this kind of spreader reduces the friction and the fiber damage commonly encountered with other methods, such as spreading bars [1]. Clemson University and the Langley Research Center have set up a recirculating powder coating apparatus in which the density of the powder cloud can be adjusted. Georgia Tech and the University of Akron use an electrostatic fluidized powder bed with a grounded tow to apply the particles. All research groups, except Clemson University, apply only convection ovens to melt the powder. Clemson utilizes a pair of electrical rollers which contact the passing tow. A voltage is applied between the rollers, inducing a current and thus heating the fibers and the powder.

The preliminary results indicate that the process is feasible, producing pregregs with a high quality in terms of uniformity and flexibility. However, only limited mechanical testing has been performed on composites made with dry coated prepregs. Thus, further evaluation of the process is needed.

CHAPTER 3

EXPERIMENTAL PROCEDURES

The complete production of carbon reinforced composites (fabrication of coated tow, mold preparation, thermo-formation) and the various tests used to characterize their mechanical properties are described in this chapter. A dry coating process was utilized to produce the prepreg, which then was laid up in molds and, finally, pressed and heated to form composites. The composites were cut into test specimens which were subjected to tensile tests, short beam shear tests, and dynamic mechanical analysis. The chapter is divided into three main parts: coating, fabricating, and testing.

3.1 Coating

In order to coat the carbon fiber tow with the polymer, a coating line, which had been built for a NASA-sponsored research project by Allen [2], was utilized. In his M.S. thesis, Allen [2] describes in detail all parts of the coating line, as well as the operating procedure. Figure 5 shows a schematic of this apparatus. In recent work the spreader used by Allen (and shown in Figure 5) was replaced [13]. Klett describes the improved spreader and modifications made to improve the reliability of the powder deposition chamber in his M.S. thesis [13]. Thus, while the schematic shown in Figure 5 correctly details the various portion of the coating line used in the present work, Klett's improved spreader and deposition chamber [13] were utilized.

The coating line consisted of four individual stages: tow movement and tension control, tow spreading, polymer coating, and polymer melting. The wind-off, the dancer arm, and the traversing wind-up provided a constant speed and tension of the tow. Both the wind-off and the wind-up spool were driven by variable speed electrical motors. The tension of the tow could be adjusted with a weight, which governed the equilibrium position of the

dancer arm. This equilibrium position could be changed by increasing or decreasing the distance between weight and pivot. The dancer arm itself was mounted on a potentiometer, which sensed the position of the arm and generated an electrical signal which controlled the speed of the take off-motor, maintaining constant tension in the tow.

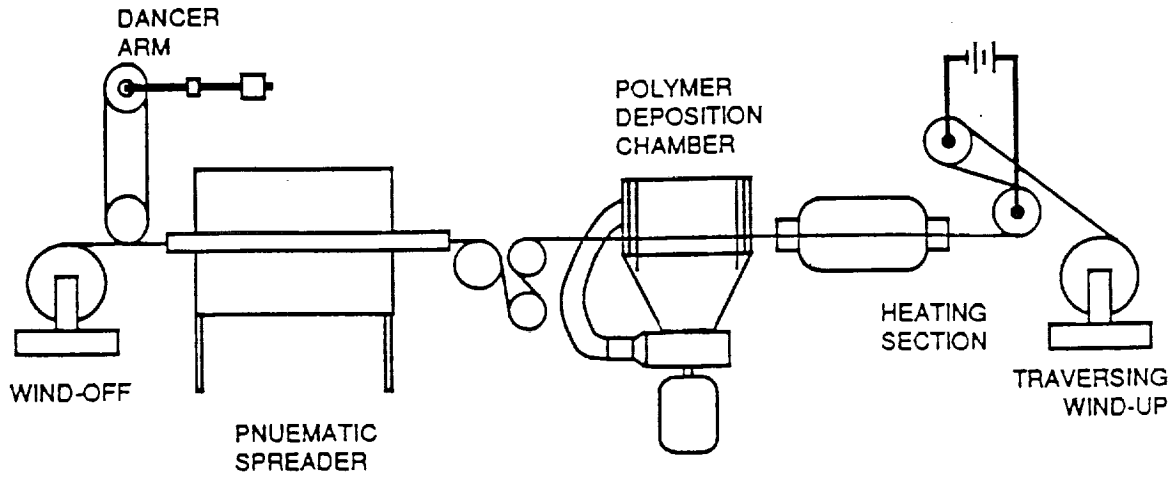

Figure 5. Schematic of coating line.

A constant tension in the tow is vital for a uniform spreading of the fibers. Tow spreading was accomplished using a new air-comb developed by Klett [13]. This device utilized pressurized air to generate a flow normal to the tow direction and expand the tow to the desired width of 7-8 cm. The air pressure in the spreader and, thus, the air flow were adjustable. Good spreading was obtained using a pressure of 0.137 MPa. After spreading, the tow entered the polymer deposition chamber, where the powder was fluidized and deposited on the tow. A polymer extruder replenished the thermoplastic resin inside the chamber during operation. A centrifugal fan mounted under the chamber maintained the constant polymer cloud density required to apply a consistent amount of polymer to the tow.

Two different types of heating sections were used to adhere the powder to the fibers (Figure 6). The first type of heating section contained a convection oven and a pair of electrical rollers. The temperature in the convection oven was limited to the minimum

necessary to eliminate build-up of polymer on subsequent electrically-charged rolls. The tow passed over these gold coated electrical contact rolls, between which a potential of 45-49 volts was applied. The potential created a current flow in the fibers, heating the fibers due to power dissipation from electrical resistance.

In the second type of heating section, only convection heating was applied to the tow. In this arrangement, a second oven replaced the electrical rollers. This was necessary in order to guarantee an adequate amount of heat to melt the powder without polymer degradation. Previous work by Allen [2] showed that if only one oven was used an extremely high temperature was needed to melt the polymer with the residence time available with a single convection oven. Indeed, decreasing the tow velocity increased the transferred heat to the tow, but the decreased speed also caused other problems in the spreading sections and in the polymer deposition chamber. Therefore, the two variations of the coating line used in the present study differed only in the heating sections, and all other parameters were kept constant. Typical process conditions used during these experiments are shown in Table 2.

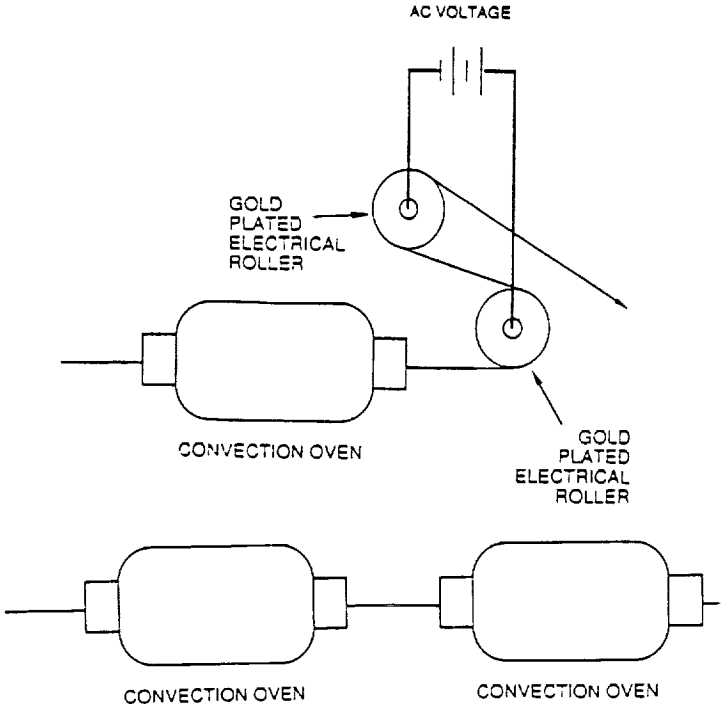

A. Convection oven and electrical rollers

B. Two convection ovens

Figure 6. Heating sections.

Table 2. Typical process conditions for coating line operation.

	two convection ovens	convection oven and electrical rollers
tow speed	3 m/min	
air pressure in spreader	0.137 MPa (5 psi on the gage)	
speed of polymer extruder	10 % of full scale	
voltage applied to the deposition chamber fan	37.8 volt (27 % of 140 volt full scale)	
temperature of oven 1	280°C	
temperature of oven 2	280°C	-
voltage between electrical rollers	-	47.6 volt (34 % of full scale)

3.2 Fabrication

Mold Lay Up

Most of the composites tested in this project were laid up in the mold, as described in the following procedure. The mold, made from A-2 tool steel, consisted of two parts, the plunger and U-shaped mold. The mold formed composites with a length of 24.1 cm and a width of a 1.3 cm. Figure 7 shows the mold and details its dimensions. The three threaded holes in the top of the plunger were used to lift the plunger following composite formation, as described in the experimental procedure. A thermocouple was inserted into the 3 mm (1/8 inch) diameter hole on the end of the plunger to estimate the composite temperature during composite formation.

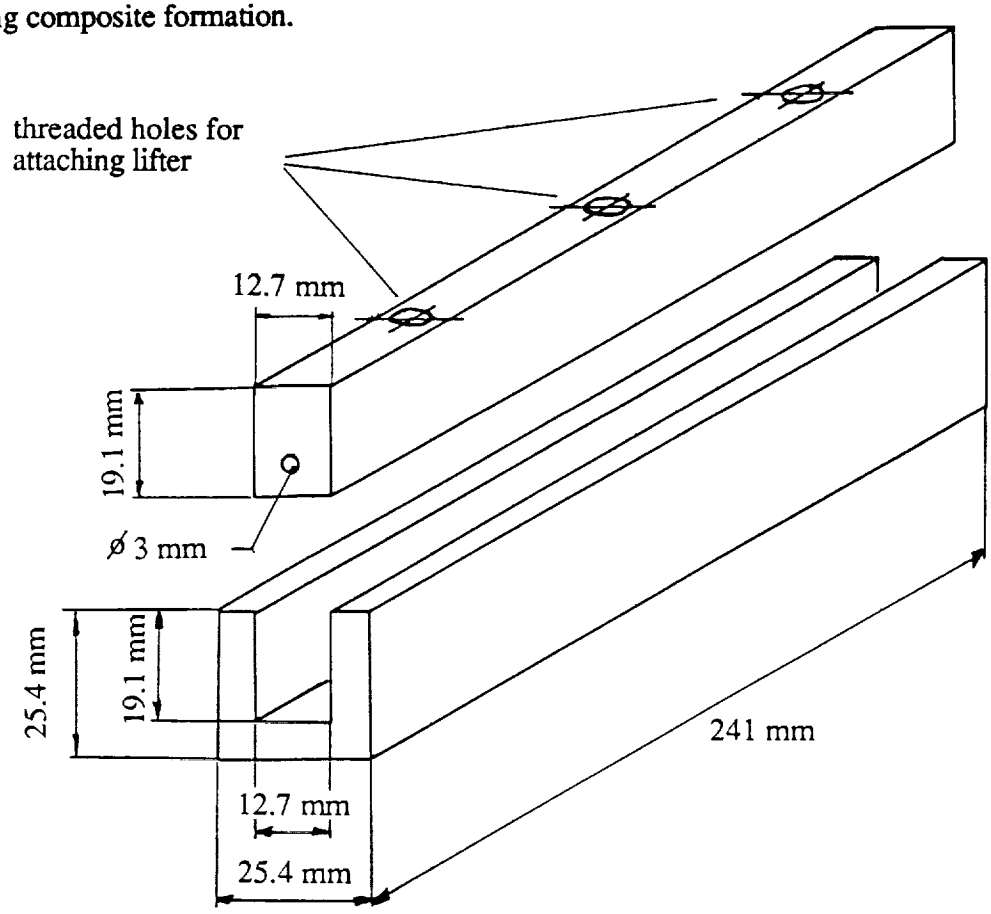

Figure 7. Mold used for all composites.

To facilitate lay up of the coated tow, a wrapping frame which was 276 mm long (Figure 8) was used.

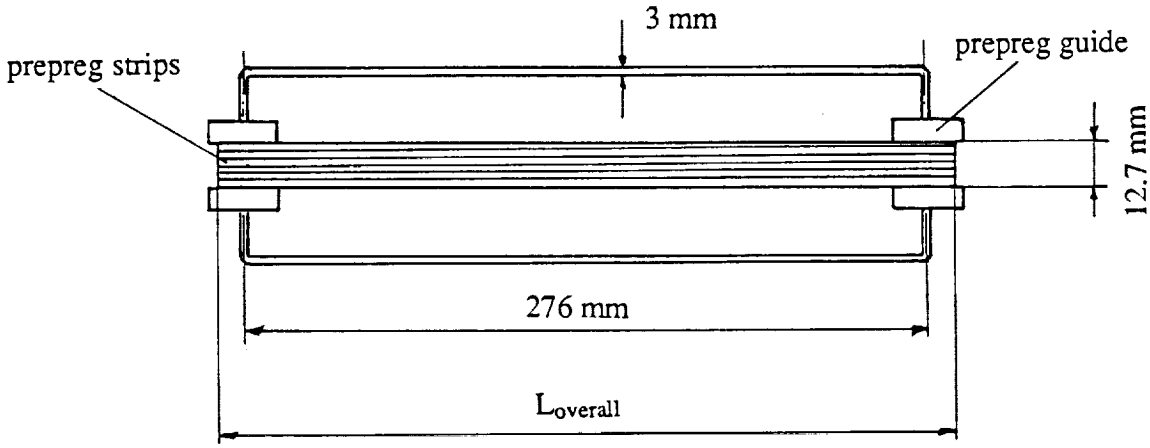

Figure 8. Wrapping frame.

1. Mount a spool with coated tow on a horizontal bar using two stands so that the spool is free to rotate. Place near the stands a balance accurate to 0.01 grams.

2. Record the combined mass of the wrapping frame and a small piece of scotch tape.

3. Using the tape, attach the end of the coated tow to one of the prepreg guides (see Figure 8) of the wrapping frame.

4. Wrap the tow across the length around the frame by rotating the frame. The strips should be gradually moved across the space between the guides so that the area is uniformly filled. Count the numbers of strips.

5. After 30 strips have been wrapped onto the frame, record the total mass of the frame and the tow to determine the overall length, $L_{overall}$, of the wrapped tow with a ruler. Do not cut the tow.

6. Calculate the number of strips needed for forming a composite with a desired cross section. (The calculation, yielding the required number of strips, is performed in the Appendix B).

7. Add the necessary strips, which can be determined by above mentioned calculation, and repeat step 4 and 5 until the ratio of the number wrapped strips to the number of theoretically required ranges between 1 and 1.03.

8. Spray the inside of the insert and the bottom of the plunger with Frekote FRP mold release and allow to dry. Repeat this procedure at least once.

9. Cut the tow from the spool and place the frame over the mold so that the tow strips lay in the U-shaped mold. Press the plunger down on the strips. Then, cut all the strips at the overlapping ends and free the frame.

Vacuum Bag

Several of the composites manufactured for this study were heated and pressed under vacuum during composite formation. In this process, a vacuum foil was wrapped around the mold, creating a bag which was sealed with a high temperature sealing tape. The vacuum foil and the sealing tape were supplied by Airtech International, Carson, California. Vacuum bagging was accomplished following the procedure below and is illustrated in Figure 9 and 10.

1. Cut a rectangular sheet of foil, 19 cm wide by 49 cm long.
2. Place the molds 2.5 cm from the edge of the foil.
3. Cut two pieces of sealing tape (27.5 cm long by 0.65 cm wide). This can be obtained by splitting 1.3 cm wide sealing tape with a razor.
4. Place the sealing tape along the edges of the foil, as indicated in Figure 11.
5. Roll four small pieces of sealing tape into balls and place them on the top corners of the mold.

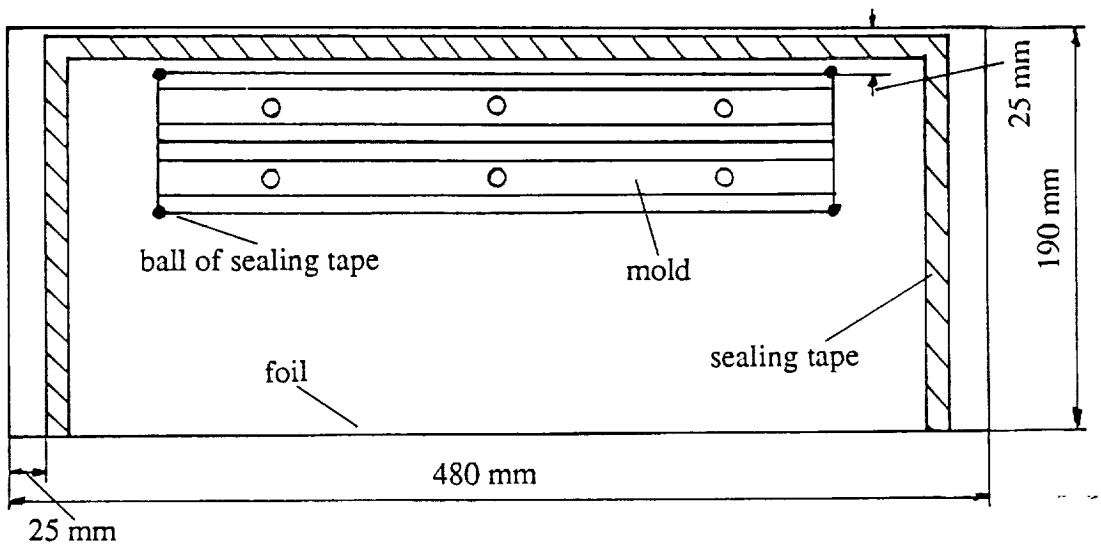

Figure 9. Illustration of vacuum bagging - step 4 (top view).

6. Wrap the foil around the molds, and seal it along the edge as shown in Figure 10.

7. Before sealing the bag at the ends, insert a 25 cm long, 3 mm outside diameter stainless steel tube in one end. Then place a K-type thermocouple in the thermocouple well of the plunger. Connect the other end of the thermocouple wire to a readout.

8. Close the ends of the tube and seal by compressing the foil against the sealing tape.

9. Connect the stainless steel tube to a vacuum pump. Test for vacuum leaks by running vacuum pump and listening for air flow into the foil bag.

10. Apply additional sealing tape, if necessary, to seal vacuum leaks.

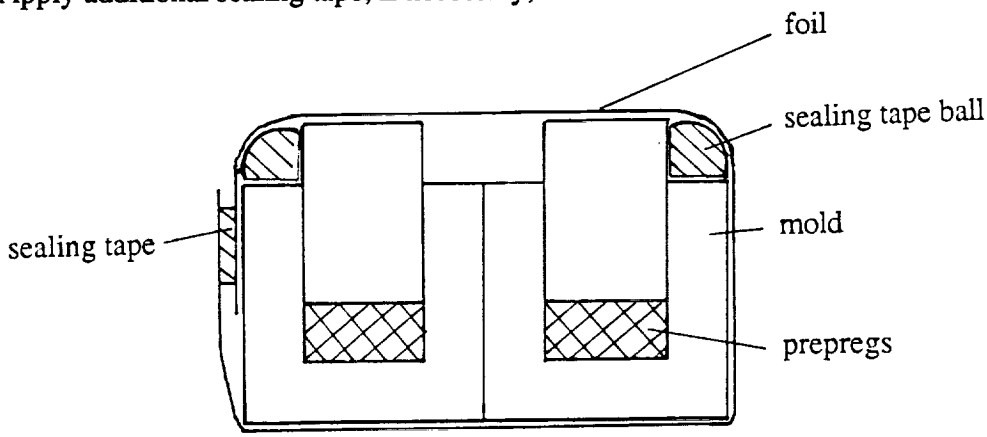

Figure 10. Illustration to vacuum bagging - step 6 (end view).

Composite Formation

Composite formation was performed by heating and pressing the molds with a high temperature Carver press. Before pressing, the bottom and the top platen of the press were preheated to 644°K. When the press reached the set point temperature, the two molds were placed in the press. For the first three minutes pressure was maintained at 0.7 MPa. Then, the pressure was increased to 6.9 MPa. This corresponded to a ram force of 42.2 KN (9500 pounds on the load gage) since the composite areas were 61.3 cm^2. After additional two minutes, the set point temperatures of the platen were reduced to 630°K, and the timer which controlled the cure time was started. Two different cure times were chosen, namely 30 min and 45 min.

At the end of the cycle, the press automatically quenched the platen to room temperature. The molds were removed from the press at the end of this quench cycle. In order to remove the composites from the mold, the three small screws on the lifter (Figure 11) were turned into the threads of the plunger. By gradually turning the stroke screws, which contacted the edge of the insert, the plunger was pulled out permitting the composite to be removed. This mold was used to prepare all test specimens used in the current study. All composites were cut into 23 cm long coupons. The flash was carefully removed with a razor blade and the rough edges were smoothed with fine sand paper.

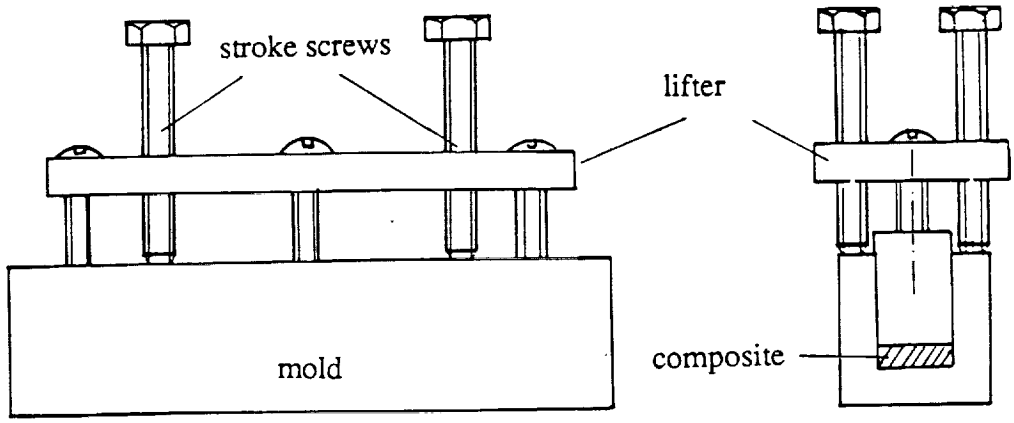

Figure 11. Lifter and mold.

Void Fraction and Fiber Fraction Calculation

To estimate the void fraction of the composites, the mass must be determined and the specimen dimensions must be accurately measured. Since the thickness is the most critical dimension, this was measured five times: at both ends, in the middle and between these points. The average thickness was used to estimate the void fraction. The following estimate agrees with the void fraction calculation by Allen [2].

The fiber volume fraction, x_{fv}, and the void volume fraction, x_{void}, were estimated using following equations:

$$x_{fv} = \frac{V_f}{V} \quad \text{, and} \tag{1}$$

$$x_{void} = \frac{V - V_f - V_p}{V} \quad , \tag{2}$$

where V = volume of test coupon,

V_f = volume of fibers,

V_p = volume of polymer.

The volume of the test coupon, V, was calculated from the following equation:

$$V = l\, w\, d \ , \tag{3}$$

where l = length of coupon,

w = width of coupon,

d = thickness of coupon.

The fiber volume, V_f, is given by

$$V_f = \frac{d_{ln}}{d_f} l\, n \quad , \tag{4}$$

where d_{ln} = 3.895E-3 g/cm, linear mass of uncoated tow,

d_f = 1.76 g/cm^3, density of the carbon fiber [14],

n = number of pregreg strips laid up in the mold.

The volume of polymer, V_p, can be estimated by:

$$V_P = \frac{W - V_f\, d_f}{d_p} \quad , \tag{5}$$

where W = mass of coupon [g],

d_p = 1.4 g/cm^3, density of LaRC-TPI [15].

3.3 Testing

3.3.1 Tensile Testing

In this test, the composite is subjected to a tensile stress in the fiber alignment direction. If ideal bonding between the fiber and the matrix is assumed, the tensile strength of the composite can be calculated using a rule of mixtures [8]. But, if there is poor interfacial bonding between the fibers and matrix, load transfer to the fibers will be poor and the tensile strength of the composite will be less than theoretical. Examination of the composites after tensile testing can give an indication of fiber-matrix bonding. If a crack forms along the fiber direction during tensile fracture, poor interfacial bonding can be assumed. A crack perpendicular to the fibers during the tensile fracture implies adequate bonding. Fiber misalignment, voids and poor matrix properties impair the performance of the specimen. Allen [2] attributed the moderate tensile strengths of LaRC-TPI/carbon composites tested during his study to a high void content, residual stresses created during composite formation, and fiber misalignment. Allen [2] reported tensile strengths of his LaRC-TPI/carbon fiber composites to be less than 890 MPa, significantly lower than the theoretical tensile strength.

In order to conduct the tensile tests in the present study, end tabs were attached to all specimens. Also, strain gages were used to determine the strain and the tensile modulus. The exact procedures followed are described below.

Figure 12 shows a typical test specimen after the end tabs had been bonded and strain gages attached. The dimensions of the test piece correspond to the dimensions of the composites used to estimate the void fraction. Therefore, no further cutting or machining was necessary.

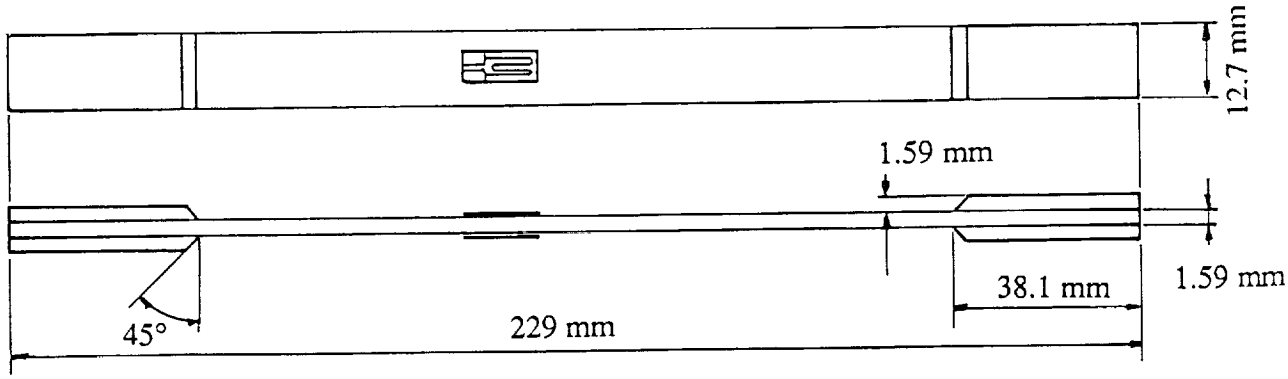

Figure 12. Tensile test specimen.

End Tab Bonding

Aluminum end tabs were glued to the specimens with EC 3569 B/A epoxy adhesive, obtained from 3M Aerospace Materials Department, St Pauls, MN. The tensile load was applied to the specimen at the bonded tabs. These tabs protected the surface of the specimen against damage caused by the scored grip surfaces. The following procedure was followed to prepare each test specimen.

1. Sand the region of the specimen where the end tabs are bonded with a medium sand paper (grade 220) in +/- 45 degree directions.
2. Clean the surfaces with acetone to remove all loose particles.
3. Cut aluminum pieces, 3.8 cm by 1.3 cm by 0.16 cm, and sand the bonding surfaces as described in step 1.
4. File one edge of the each tab to a 45 degree angle (see Figure 12).
5. Clean the surface of the tabs with acetone.
6. Separate a small amount of the white resin EC 3569B, determine its mass and blend it with the adhesive accelerator EC 3569A until it attains an uniform green color. The mixing ratio is two parts, by mass, of the white resin to one part, by mass, of the accelerator. Two grams of this blend is sufficient to bond 30 cm^2.
7. Apply the mixed adhesive with a spatula to the prepared surfaces of the specimen.
8. Align the end tabs on the specimen and press them down so that any superfluous adhesive is squeezed out.
9. The cure time for the adhesive should be at least 24 hours.

Strain Gage Bonding

In order to determine the tensile modulus of the composites, strain gages were attached to the specimen. The strain gages, supplied by the Measurement Group Inc., Romulus, Michigan, have a resistance of 120 ohms and a gage factor of 2.05. The performance of the gages is absolutely dependent on the bond between the gage and the specimen. Only a perfect bond guarantees an undiminished transmission of strain between the test piece and the gage. The procedure used to apply the strain gages follows that given in the Student Instruction Bulletin of the Measurement Group Inc [16].

1. Use acetone applied to a tissue to degrease the center of the specimen.
2. Place a liberal amount of M-Prep Conditioner A in the gaging area, and abrade the surface lightly with a fine [180, 220 grit] silicone carbide paper.
3. Dry the surface with a clean tissue.
4. Apply several drops of M-Prep Neutralizer 5, and scrub the surface with a clean cotton tipped applicator.
5. Dry the surface with a clean tissue.
6. Draw a reference line normal to the length of the composite with a pencil in the desired area.
7. Remove the strain gage from its envelope with tweezers and place it bond side down on the empty gage box.
8. Anchor one end of a clear plastic tape piece (8 cm long) on the gage box behind the gage, and wipe the tape down over the gage. Pick up the gage by lifting the tape.
9. Position the gage on the sample using the reference line and attach the tape.
10. In preparation for applying the adhesive lift one end so that the bonding side of the gage is exposed. Tack the loose end of the tape.
11. Apply the M-Bond 200 Catalyst on the gage with the bottle brush.
12. Place one or two drops of M-Bond 200 Adhesive at the junction of the tape and the specimen surface. Reposition the gage on the specimen and set the gage in place using a tissue to press over the gage tape assembly.

13. Press your thumb on the top of the gage for one minute.
14. Turn the specimen to the other side and repeat the process for the second gage.
15. Remove both pieces of tape and solder thin lead wires to the gage. To prevent strain on the gages from the wire, wrap a piece of tape around the specimen and the wires.
16. Record the resistance of the strain gages and the connecting wires.

Testing Procedure

The tensile tests were conducted on an Instron 1125 testing machine, according to the ASTM D 3039-76 procedure [17]. The load cell used for these tests has a capacity of 10,000 kg. The samples were placed in the Instron between the two wedge grips of the Instron and carefully aligned. The wires of the strain gages were connected to the corresponding terminals of a Wheatstone bridge, as illustrated in Figure 13:

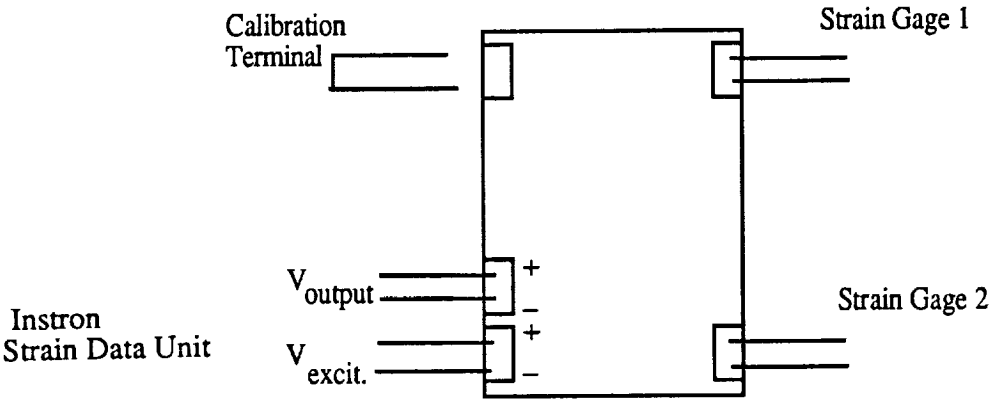

Figure 13. Connection schematic of Wheatstone bridge.

The Wheatstone bridge was designed and built to interface between the strain gages and the Instron strain data recorder. It should be noted that only strain gages with a resistance

of 120 ohms were compatible with this bridge. In order to calibrate the Wheatstone bridge with the connected strain gages, the pen of the plotter, which records the signal from the strain data unit, was set to zero. The calibration terminal was closed, causing the pen to deflect. This deflection was adjusted to full-scale with the calibration knob. This corresponds to a given strain which can be calculated (see Appendix A). The load cell was calibrated with the load cell amplifier. The full-scale deflection of the plotter corresponded to a 5000 kg load.

The specimen was strained at a constant crosshead speed of 2 mm/min. The plotter recorded the load, as well as the strain, versus time. Both the tensile strength and the tensile modulus were determined by analyzing the plot. The peak of the load curve was noted as breaking load, L_{max}. This load, L_{max}, divided by the minimum cross section area of the specimen yields the tensile strength:

$$\sigma = \frac{L_{max}}{b\,w} \quad , \tag{6}$$

with L_{max} = maximum load [N],

w = width of specimen [m],

b = thickness of specimen [m],

σ = tensile strength [Pa].

The tensile modulus is defined as:

$$E = \frac{\sigma}{\varepsilon} \quad , \tag{7}$$

with E = tensile modulus [Pa],

σ = applied tensile strength [Pa],

ε = generated strain [-].

It should be noted that carbon fiber reinforced composites can be considered perfectly elastic over their test range, thus, the modulus remains constant. During tensile testing tensile modulus can be determined as follows:

$$E = \frac{\Delta\sigma/\Delta t}{\Delta\varepsilon/\Delta t} \quad , \tag{8}$$

with $\Delta\sigma$ = change of tension [Pa],

$\Delta\varepsilon$ = change of strain [-],

Δt = time interval [s].

With the plot of load and strain versus time, equation 8 can be employed to determine the tensile modulus . The determination of the tensile modulus is performed in Appendix B.

3.3.2 Short Beam Shear Testing

This test method determines the apparent interfacial shear strength of unidirectional fiber reinforced plastics. The specimen is a short beam formed either by cutting samples from ring-type specimen or by fabricating a flat, unidirectional sample up to 6.4 mm in thickness [18]. During the test, the specimen ends rest on two supports to allow lateral motion. Then, a load is applied, using a loading nose centered at the midpoint of the specimen. Figure 14 shows the geometry of the rectangular short beam shear test.

In order to get a pure shear failure mode, the bending moment in the beam must be low and the transverse load sufficiently high. This can be achieved when the span-to-length ratio is low. For carbon fiber reinforced plastics, a span-to-length ratio of four and a length-to-thickness ratio of six are recommended. However, Banerjee [19] conducted short beam shear tests on carbon-epoxy composites with the recommended ratios and reported the occurrence of mixed failures, i.e., a combination of a compression/tension mode and a shear failure mode. Therefore, it is important to identify the failure mode after

testing, since only a failure in the pure horizontal shear yields the apparent shear strength. Figure 15 [20] illustrates the failure modes possible when a specimen is subjected to a short beam shear test. It should be noted that the apparent interfacial shear strength obtained in this test is only used for comparative testing, not for developing design criteria.

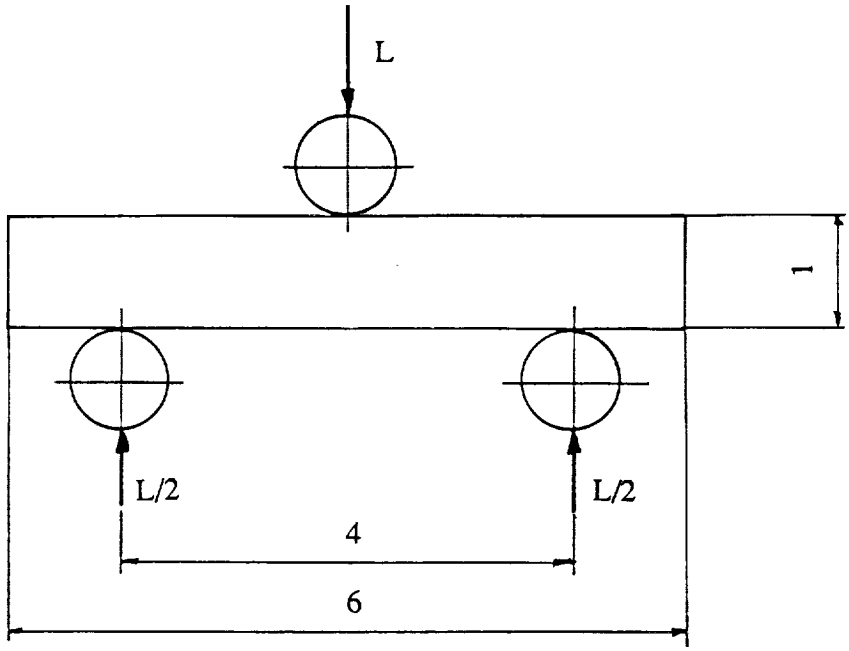

Figure 14. Load diagram and test specimen with recommended dimension ratios.

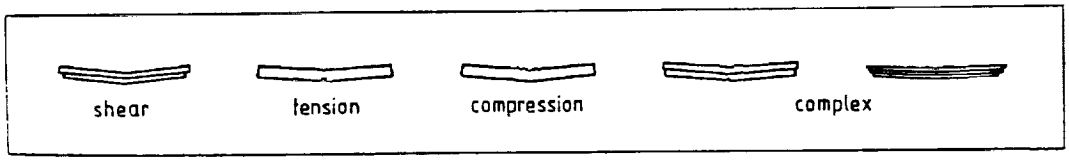

Figure 15. Possible failure modes of the SBS test.

The short beam shear properties reported in the literature for LaRC-TPI/carbon fiber composites vary considerably. Having tested LaRC-TPI/AS-4 Hercules composites made using a slurry technique followed by pultrusion, the Central Research Laboratory of the Mitsui Toatsu Chemicals, Inc. [21], reported a interlaminar shear strength of 124 MPa at

room temperature. Similar composites prepared by NASA, also consisting of LaRC-TPI and AS-4 fibers, failed in shear at 86 MPa [12]. These composites were made using a dry coating process and were formed with a heating press. This seems to indicate that the interlaminar shear strength is strongly dependent on the technique used to form the specimen.

In the present study SBS testing was conducted according to ASTM Standards D 2344-84 [18]. As recommended for carbon fiber reinforced composites, a span-to-depth ratio of four and the length-to-span ratio of six was employed. The test fixtures were held by the grips of a universal testing machine, which was used to apply the load. The dimensions of the specimen were 1.9 cm by 1.27 cm by 0.315 cm (Figure 16). The specimens were cut from 22.9 cm long bars which had been fabricated in the same manner as the specimens for the tensile testing.

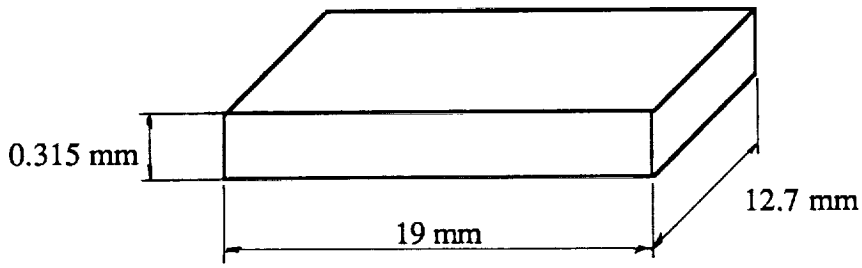

Figure 16. Test specimen dimensions.

The fixture utilized for SBS testing is described by Banerjee [19] and Diwan [22]. The frame (detailed by Diwan [22]) was held with two L-shaped aluminum pieces connected by two threaded bars (Figure 17). An aluminum plate was placed under the frame to protect the surface of part B. The loading nose employed for SBS testing is detailed by Banerjee [19].

This configuration provided a span of 1.27 cm corresponding to the recommended 4:1 ratio between the span and the thickness of the specimen. After this fixture was mounted in the Instron testing machine, the pins in the frame and the pin of the upper part were aligned parallel. Then, the specimen was positioned on the lower pins. Care was taken that the specimen was aligned with the fixture. Before starting the test, the cross-head speed was adjusted to 1.0 mm/min and the plotter was switched on. The plotter recorded the load versus deformation curve. After the test, the breaking load was noted by marking the maximum load during deformation.

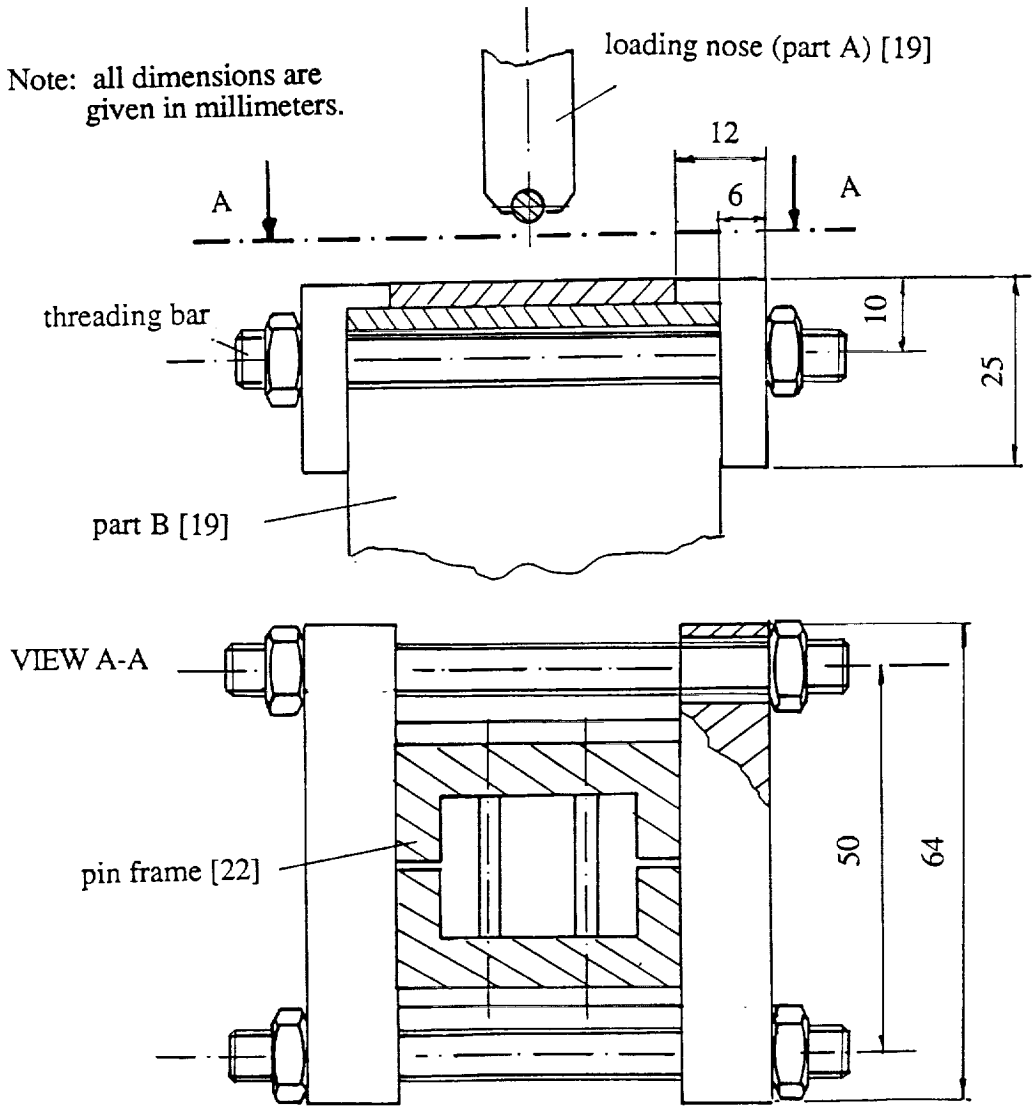

Figure 17. Fixtures used for SBS test.

The apparent interfacial shear strength , τ , was calculated by:

$$\tau = 0.75 \frac{L}{b\,d} \quad , \tag{9}$$

where L = Load [N],

b = width of test specimen [m],

d = thickness of test specimen [m].

At the completion of testing, the average shear strength and the standard deviation of the specimens which failed in true interfacial shear were determined.

3.3.3 Dynamic Mechanical Characterization

Dynamic mechanical analysis can be used to characterize the interfacial bond strength of composites materials and is the only non destructive test available to study the fiber matrix interface [19]. Banerjee [19] conducted dynamic mechanical characterization tests to determine the viscoelastic behavior of epoxy-carbon composites and measured the energy dissipation at the fiber/matrix interfaces which occurred during dynamic testing. Cano [23] used the same method to detect the difference in fiber/matrix bonding between composites fabricated using PAN-based and pitch-based carbon fibers, as well as to differentiate between composites consisting of the same matrix material and pitch-based fibers with different moduli.

Dynamic mechanical characterization is based on the different fundamental responses of viscous and elastic elements to a sinusoidally varying stress or strain. If a sinusoidal strain of the form

$$\gamma = \gamma_0 \sin \omega t \tag{10}$$

is applied to a viscoelastic specimen (γ_0 is the amplitude and the ω is the angular frequency), the resulting stress is also sinusoidal, but is out of phase and can be written in the form:

$$\sigma = \sigma_o \sin (\omega t + \delta) \quad , \tag{11}$$

where σ_0 is the maximum amplitude of the stress. Thus, the stress lags behind the strain by a phase angle δ. For a purely viscous material, δ would equal 90^0, while for a purely elastic material δ equals 0^0. For a viscoelastic material, such as a polymer matrix material, the δ lies between 0^0 and 90^0. It can be shown that for a purely elastic material the deformation energy is completely stored because the stress and strain always lie in phase. On the other hand, for a purely viscous material all deformation energy is dissipated in the form of heat. For a composite consisting of fibers (pure elastic), a polymer matrix (viscoelastic) and a fiber matrix interface, the deformation energy is mainly dissipated in the matrix and the interface. Thus, composites with poor interfacial bonding tend to dissipate more energy than composites with good bonding.

Equation 11 can be expanded to yield the following:

$$\sigma = \sigma_0 \cos \delta \sin \omega t + \sigma_0 \sin \delta \cos \omega t \quad . \tag{12}$$

With the aid of equation 12, one can see that the resulting stress can be divided into two parts: one which is in-phase with the applied strain, and one which is out-of-phase. As one might suspect, the analysis of this response often utilizes a complex representation with a real part (in-phase) and an imaginary part (out-of-phase). In this form, the complex strain, γ^*, is given by:

$$\gamma^* = \gamma_0 e^{i\omega t} \quad , \tag{13}$$

with i is an imaginary number. The corresponding complex stress, σ^*, with a phase difference, δ, can be written as:

$$\sigma^* = \sigma_0 e^{i(\omega t + \delta)} \quad . \tag{14}$$

The complex shear modulus is the quotient of the complex strain and the complex stress:

$$G^* = \frac{\sigma^*}{\gamma^*} \quad . \tag{15}$$

Using mathematic transformations, this leads to the equation:

$$G^* = G' + i\,G'' = \frac{\sigma_o}{\gamma_o}\, e^{i\delta} = \frac{\sigma_o}{\gamma_o}\sin\delta + i\frac{\sigma_o}{\gamma_o}\cos\delta \quad . \tag{16}$$

Thus, we find that

$$\tan\delta = \frac{G''}{G'} \quad , \tag{17}$$

where G' is defined as the shear storage modulus and G" is the shear loss modulus.

The dynamic mechanical characterization of the composite samples was conducted using a RDS 7700 dynamic spectrometer. The samples were tested in a torsional shear mode to measure the shear storage modulus, G', and the shear loss modulus, G". The typical dimensions of the test specimens were 63.5 mm by 12.7 mm by 1.6 mm (Figure 18). They were cut from 22.9 cm long bars, fabricated according to the composite formation procedure described earlier.

Initially, a strain sweep was conducted to determine the range of strains over which the specimens exhibited linear viscoelastic behavior. Then a maximum strain of 0.1% was selected (to ensure linear behavior during all tests), and tests were conducted over frequencies ranging from 0.1 to 25 rad/s. The high level of torque, characteristic of composites, increased accuracy of the measurement.

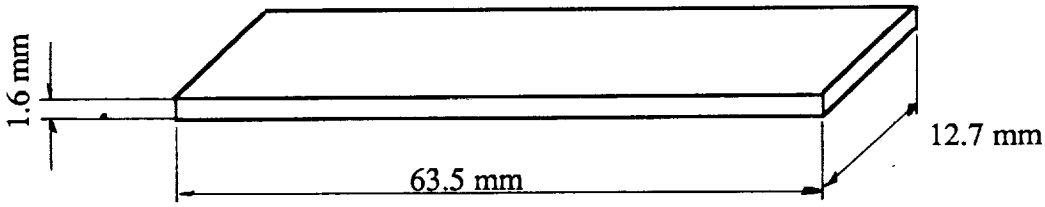

Figure 18. Test specimen for dynamic mechanical characterization.

The procedure followed to determine the dynamic mechanical properties of the composite specimens on the Rheometrics RDS 7700 spectrometer was as follows:

1. The air valve was opened after making sure that the inlet air was completely dry.

2. The main power was switched on and the motor and the transducer were started.

3. Two U-shaped inserts were placed on each end of the 64 mm long composite sample. If the fixture did not fit tightly, shim stocks were used to fill the gap between the sample and the inserts.

4. The length between the fixtures, as well as the width and the thickness, were measured with a micrometer.

5. The Geometry Selector Switch, as shown in the computer front view (Figure 19) was moved to the torsion geometry rectangular mode.

6. The Test Geometry button was pressed and composite dimensions, in millimeters, were entered into the system via an IBM PS/2 computer terminal.

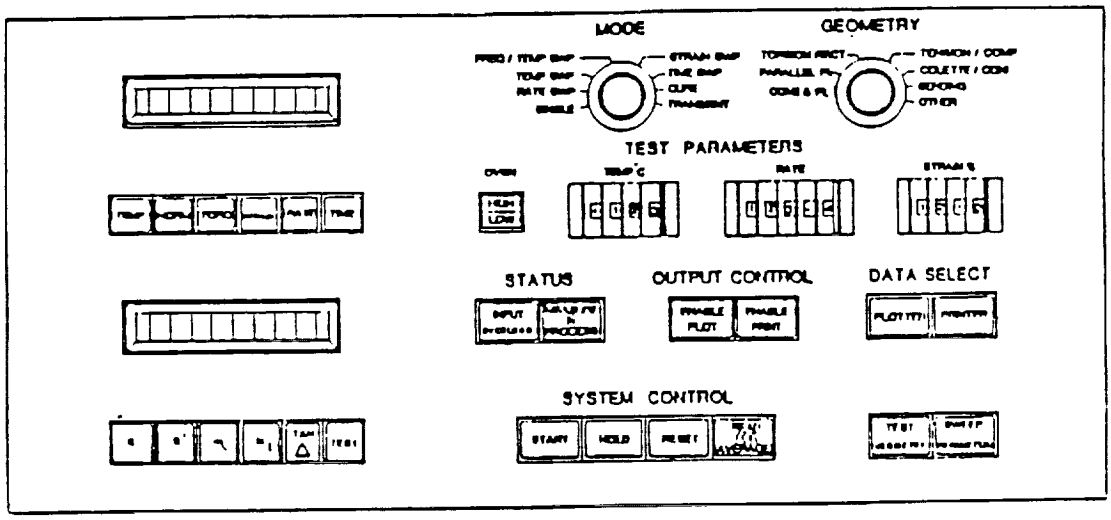

Figure 19. Front view of Rheometrics RDS-7700 auxiliary control panel.

7. The sample was then attached to the lower test fixture by tightening the set screw of the collar (Figure 20).

8. The upper grip was lowered using the platform controls, shown in Figure 21, so that it touched the upper end of the sample, care being taken not to overload the transducer. The contact between upper test fixture and the sample was indicated by a rightward deflection of the normal force meter.

9. The sample was attached with the other collar to the upper test fixture.

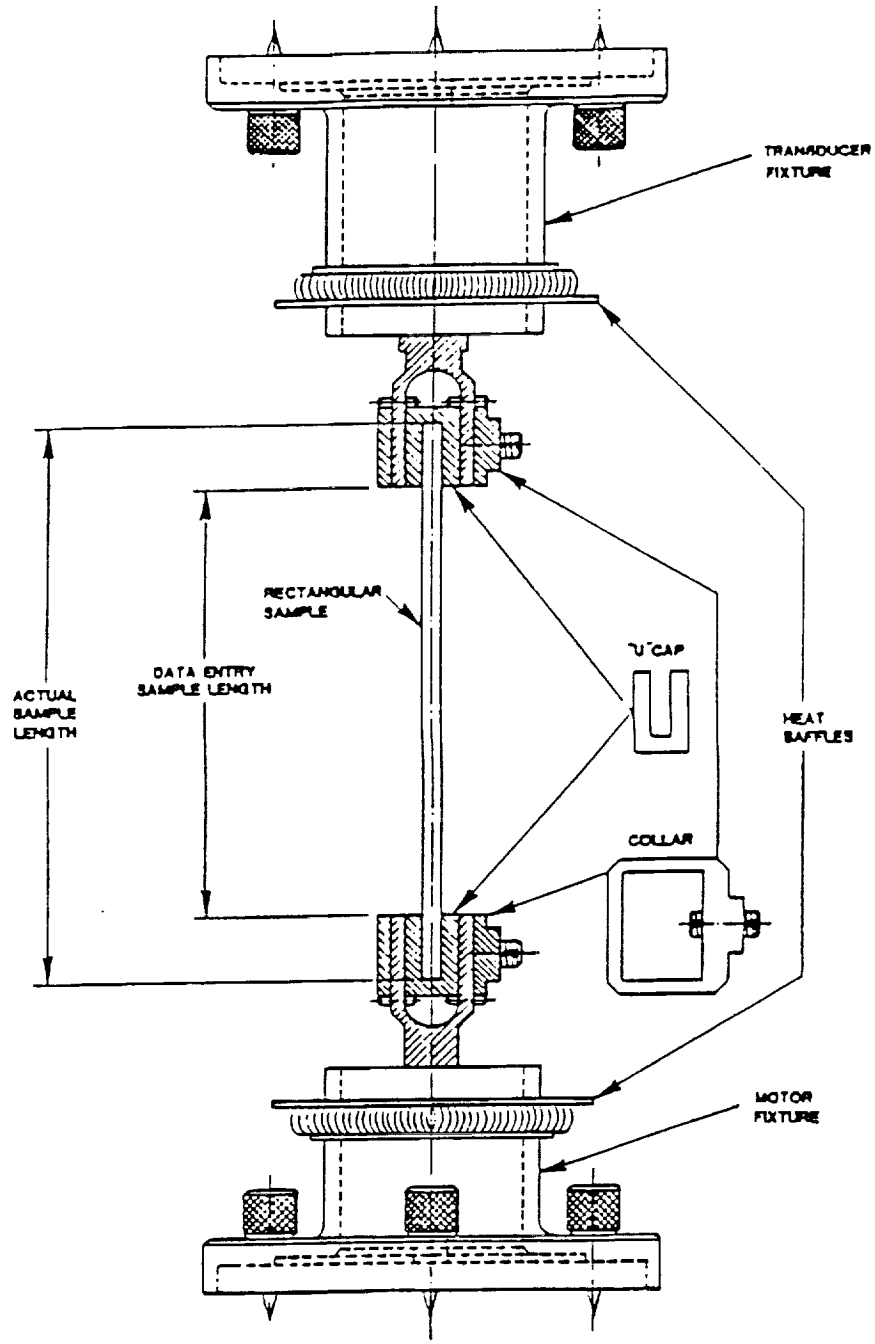

Figure 20. A typical dynamic mechanical test specimen mounted in the rectangular torsion test fixture.

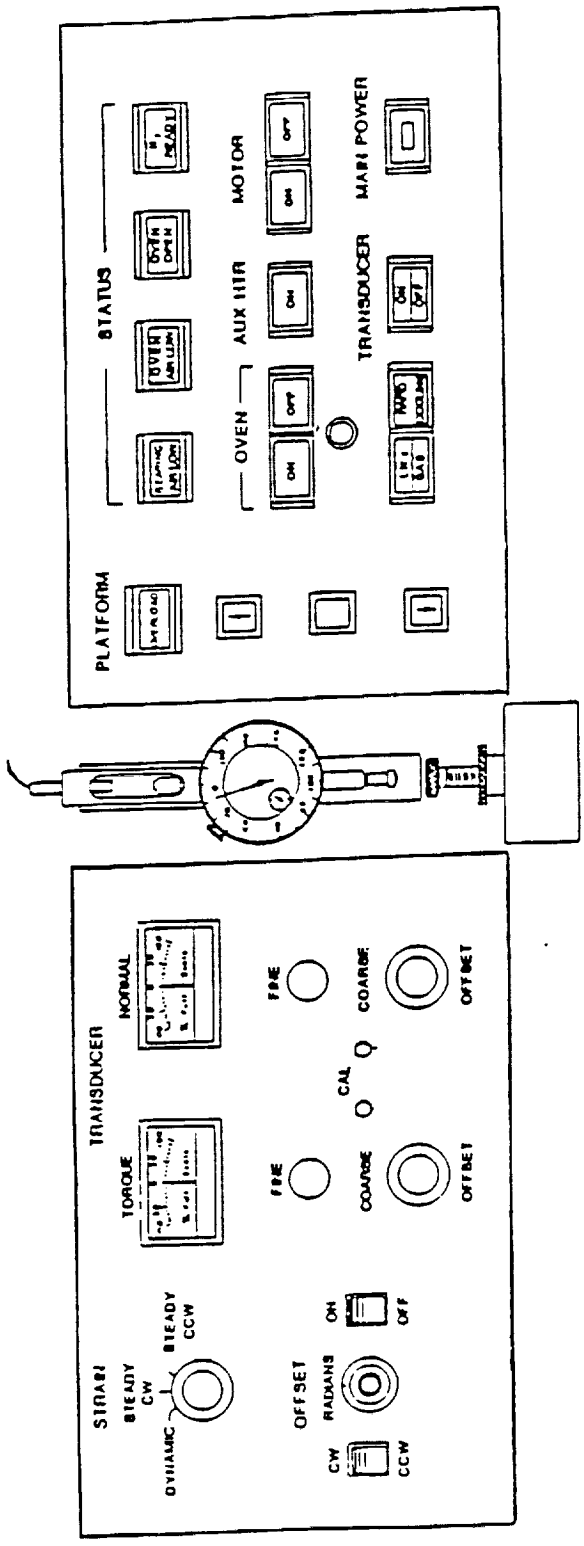

Figure 21. Test station main control panel.

10. In order to avoid buckling during testing, a normal tensile force of was applied by raising the platform until the normal force meter read a tension force of 10-15%.

11. To measure the storage modulus, G', the loss modulus, G", and the tan δ , the spectrometer was operated in the rate sweep mode. Thus, the mode selector switch was set to Rate Sweep.

12. The rate selector thumbwheel switch was moved to read 0.1 rad/s, the strain percentage thumbwheel switch was adjusted to indicate 0.1%.

13. The Sweep Geometry button was pressed and information regarding correlate delay, the number of points per decade, and last rate were supplied. The number of points per decade selected was five, the correlate delay chosen was three seconds, and 25 rad/s was chosen as the last rate.

14. Finally, the test was started by pressing the Start button and the Enable-Print button was activated to allow the G' and G" data to appear on the computer screen.

All data were stored by the attached computer and could be subsequently printed and plotted for evaluation. During the dynamic test, the servo-motor of the spectrometer applied a sinusoidal strain to the specimen, the test specimen responded with a sinusoidal stress, which was measured by the transducer. The G', G" and tan δ were calculated by the computer. First, the computer calculated the geometric scaling factor, K, as

$$K = \frac{980.7\,L}{\left(\frac{d}{10}\right)^3 b\left(0.33 - 0.21\,\frac{d}{b}\right)} \quad , \tag{18}$$

where L is the test length of the sample, b the width of the sample and d is the thickness of the sample. The strain, γ, was calculated as

$$\gamma = \frac{\Theta\, d}{L} \quad , \tag{19}$$

where Θ is the imposed angle of deflection in radians. The loss modulus, the storage modulus and the dynamic complex modulus G* were obtained as follows:

$$G' = K\left(\text{Real}\,\frac{M}{\Theta}\right) \quad , \tag{20}$$

$$G'' = K\left(\text{Imag}\frac{M}{\Theta}\right) \quad , \tag{21}$$

and

$$G^* = \left[(G')^2 + (G'')^2\right]^{1/2} \quad . \tag{22}$$

Here M is the torque measured by the transducer, Real (M/Θ) is the in phase component of torque divided by the imposed strain, and Imag(M/Θ) is the out of phase component. Finally, the loss tangent δ was given as

$$\tan\delta = \frac{G''}{G'} \quad . \tag{23}$$

All calculations described above were performed by the Rheometrics data-reduction computer. For each series of test, the average of G', G", and tan δ, along with the corresponding standard deviations were calculated.

CHAPTER 4

RESULTS AND DISCUSSION

As described in Chapter 3, more than 1500 meters of prepreg were produced with the coating line. Nearly two thirds of this amount were made using the one convection oven and the electrical rollers (pregreg A), the other third was obtained utilizing two convection ovens (pregreg B). The two different pregregs were used to lay up composites which then were pressed and heated in a heating press to form composites. Two parameters of the consolidation, namely the cure time and the use of vacuum, were varied for the composites made from prepreg A. Tensile tests, short beam shear tests, and dynamic mechanical tests were conducted to characterize the mechanical properties of these composites.

This chapter is divided into three primary sections: prepreg characterization, results of void fraction calculation, and results of mechanical tests.

4.1 Pregreg Characterization

Since both prepreg A and prepreg B were flexible, the coated tows could be wound around the wrapping frame. Often prepreg A and prepreg B had a nonuniform, mottled appearance. This can be attributed to the agglomeration of the fine LaRC-TPI powder into clumps, and probably resulted from moisture in the extruder and deposition chamber. Nevertheless, these clumps appeared to melt adequately during processing. During the formation of the prepreg tow, powder adhesion was evaluated by gently rubbing the tow. If powder particles could be removed from the tow by rubbing, adhesion was considered to be poor. All the prepreg tows produced for this study had excellent adhesion when evaluated in this manner. Figures 22 and 23 are scanning electron micrographs from prepreg A and B. These figures show that individual polymer particles melted on the fibers. The contact areas between the single powder particles and the filaments were

slightly larger for the prepreg B, indicating that the powder was more completely melted when two ovens were employed. Since the initial yellow LaRC-TPI powder becomes dark

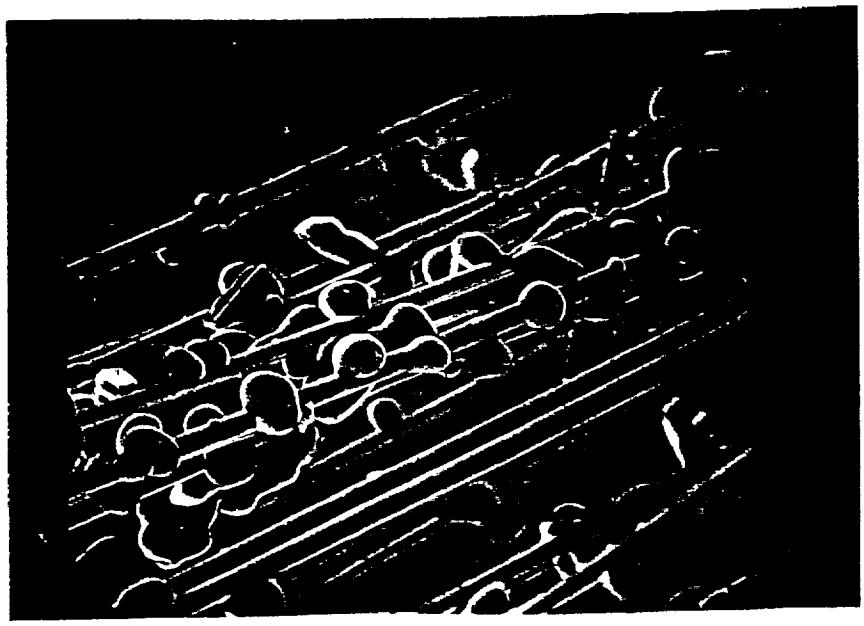

Figure 22. Scanning electron micrograph of prepreg A.

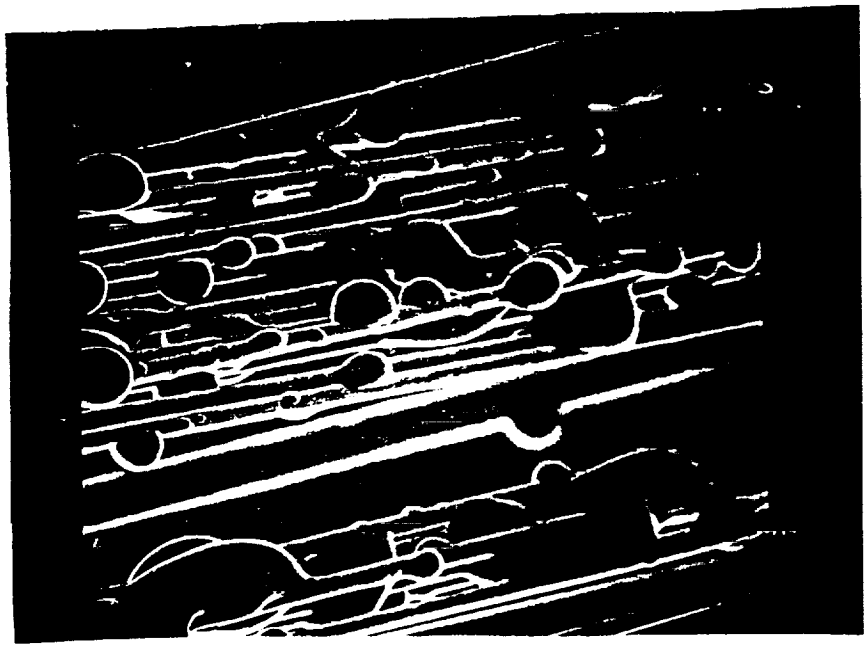

Figure 23. Scanning electron micrograph of Prepreg B.

when it is melted, another indication that more heat was applied was the darker appearance of prepreg B in comparison with prepreg A. In summary, the coating line with either heating systems produced prepregs which were sufficiently flexible to allow an easy handling.

4.2 Results of Void Fraction Calculation

Almost 75% of all composites made in this work contained a void fraction of less than 5%. Allen [2] reported void fractions between 5% and 13% using a similar coating line with electrical rollers. The lower void content of the composites produced in the present work can be attributed to an improved composite consolidation procedure. Figure 24 shows the thermal history of typical composites produced in this study (with two different cure times) and in the study conducted by Allen [2].

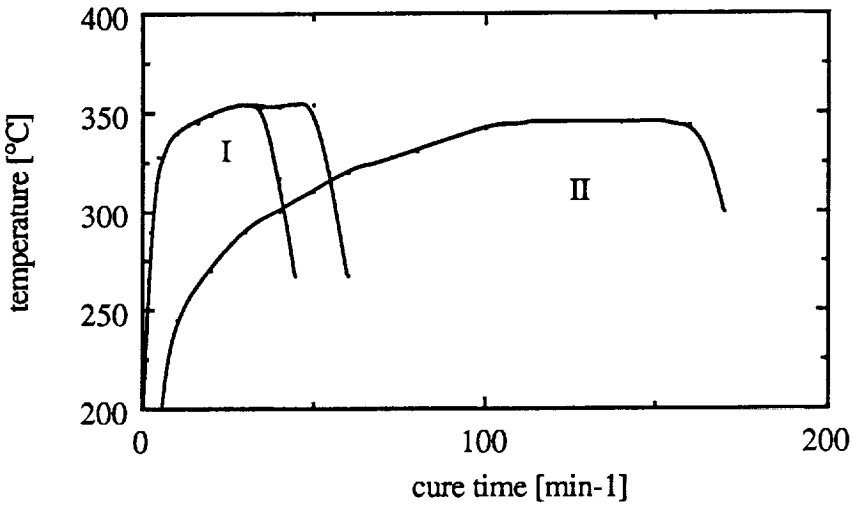

Figure 24. Thermal history of consolidation. I - present work, II - Allen [2].

The temperature was measured using a type J thermocouple inserted in the thermocouple well in the mold. LaRC-TPI has a time-dependent melt viscosity (see Figure 3 in Chapter 2), and after 10 minutes at typical processing temperatures, the viscosity rapidly increases by several orders of magnitude. Therefore, the heat-up time must be short to take advantage of the low viscosity. The difference in the heat-up times between this work and Allen's study can be explained by the lower weight of the mold mass. The lower mass, and thus, the smaller heat capacity of the mold, improved the heat-up time. However, several composites contained a void content greater than 10%. For example, samples 23 and 24, which were formed side-by-side, had a void fraction greater than 13%. The likely cause for this was the high fiber fraction (74%) of the sample 23. Even coating becomes more difficult as the fiber fraction increases. When the matrix material does not surround the fibers evenly, air can be trapped in the composite as voids, causing the final composite thickness to be greater than expected. The thickness of sample 23 was 0.195 cm instead of the expected value of 0.159 cm. The thickness of sample 24 was also greater than expected, 0.188 cm, but, it was less than the thickness of sample 23. The specimen thickness is very critical when two samples are processed side-by-side because it influences the pressure distribution among the composites. Since the platens of the press remain parallel during processing, most of the applied force will act on the sample with the greater thickness. Therefore, sample 23 was actually processed at a higher pressure than sample 24. The low pressure in sample 24, which had a moderate fiber volume fraction, probably was not adequate to minimize voids.

The results of the void fraction evaluation between prepregs A and B, as well as between the composites made with different consolidation parameters, are illustrated in Figures 25 and 26. Figure 25 compares the void fractions of the composites formed from two different prepregs. More than 80% of the composites made with prepreg B contained less than 2.5% voids, and all composites of this group exhibited void fractions less than 5%. One reason for this smaller void fraction could be that prepreg B was exposed to more

heat as it passed through the two convection ovens. This may have removed moisture and other volatiles more efficiently during prepreg formation, decreasing bubble formation during composite processing. In order to verify this assumption, neat LaRC-TPI powder was removed from the extruder and then pressed and heated under the same conditions used to form the composites from prepreg B. Indeed, bubbles could be seen in this specimen.

Figure 26 shows how the cure time and vacuum effect the final void fraction of the composite. Neither the extension of the cure time nor vacuum reduced the void fractions significantly below that of the composites cured for 30 minutes.

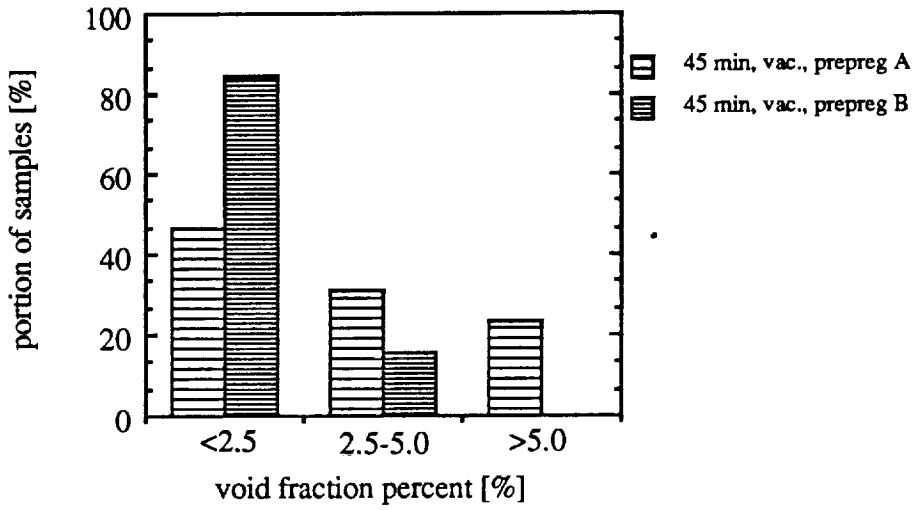

Figure 25. Void fraction of composites made from prepreg A and B.

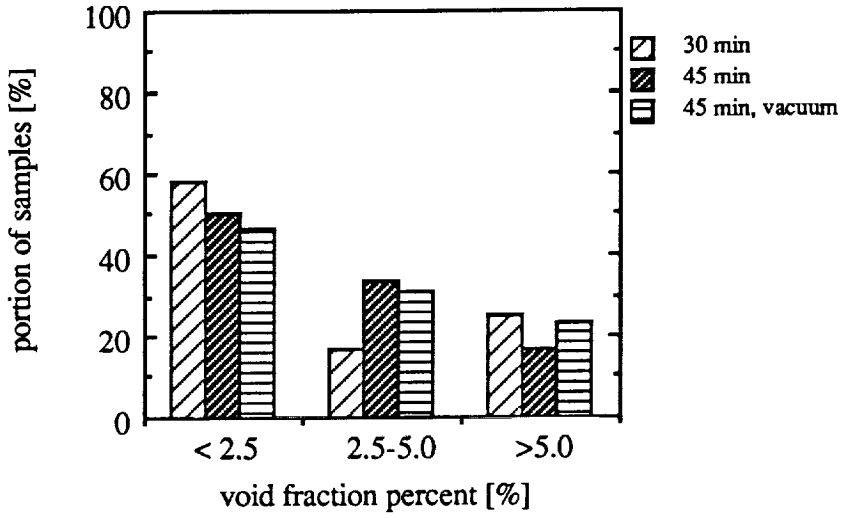

Figure 26. Influence of consolidation parameters on void fraction (prepreg A).

4.3 Results of Mechanical Tests.

4.3.1 Tensile Test

Tensile tests were conducted on 36 test specimens: 9 specimens were made from prepreg B, and the remainder were formed from prepreg A. The specimens formed from prepreg A consisted of three different groups of nine samples processed under different conditions: namely, 30 minutes cure time, 45 minutes cure time, and 45 minutes cure time under vacuum. The tests were conducted according ASTM D 3039-76 [15] and are described in Chapter 3. The tensile strength data and standard deviations are listed in Table 3 for the four composite groups.

Table 3. Tensile strength data.

	cure time [min]	vacuum [-]	tensile strength [MPa]	fiber fraction [%]
prepreg A (electrical rollers)	30	-	955±166	59±7.1
	45	-	905±251	61±9.5
	45	used	984±281	57±7.7
prepreg B (two convection ovens)	45	used	1082±132	56±9.0

± denotes standard deviation.

The average tensile strength of the three groups of composites made with prepreg A were not significantly different (based on student-t test and the 80% confidence limits). When composites formed under similar cure conditions but from different prepreg are compared, again the average tensile strength is not statistically different. Assuming the rule of mixtures applies [8], one would expect a high standard deviation in the measured tensile strength when fiber volume fraction varies. Scatter caused by variation in fiber volume fraction can be removed by computing a normalized tensile strength, σ_n. The normalized tensile strength, σ_n, is the tensile strength of the composite, σ, divided by the product of its fiber volume fraction, x_{fv}, and the strength of the fiber [14], σ_{fib} (the tensile strength of the matrix is neglected). Thus, the normalized tensile strength, σ_n, is calculated as:

$$\sigma_n = \frac{\sigma}{x_{fv}\,\sigma_{fib}} \quad . \tag{24}$$

Surprisingly, the coefficients of variation of the normalized tensile strengths for the individual groups were even larger than the coefficient of variation of the original tensile

strength data listed in Table 3. To explain the reason for this, the normalized tensile strength, σ_n, is plotted as a function of the fiber volume fraction in Figures 27 and 28.

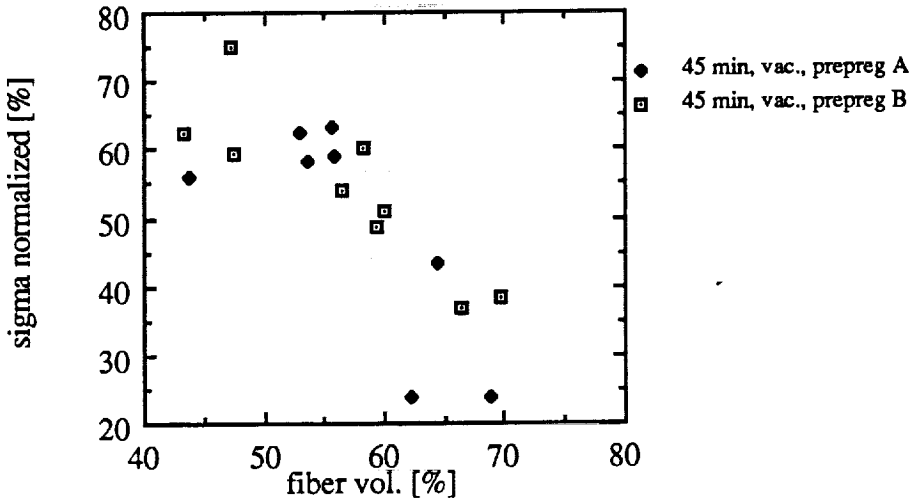

Figure 27. Normalized tensile strength of composites formed from different pregregs and consolidated under similar conditions.

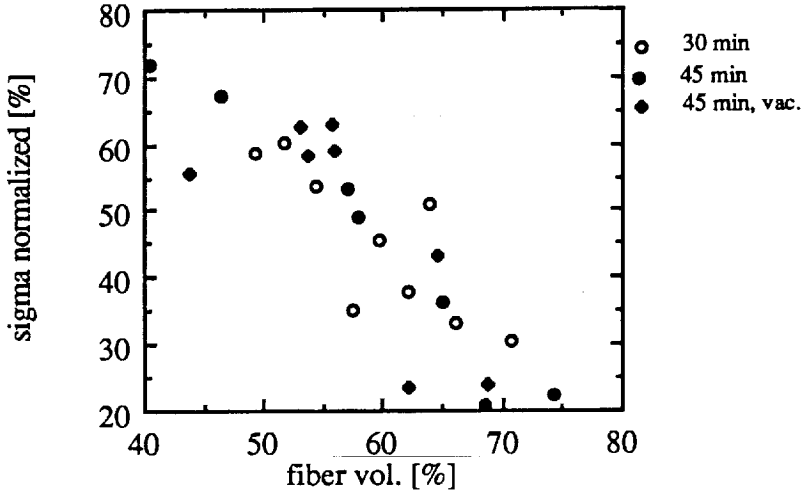

Figure 28. Normalized tensile strength of composites formed with the same prepreg and consolidated under different conditions.

The normalized tensile strength decreased with increasing fiber volume fraction for all groups. No significant difference can be seen, either between composites formed from prepreg A and prepreg B, or between different consolidation conditions. This indicated, that the tensile strength data were insensitive to both the prepreg type and the exact consolidation conditions employed during composite formation. However, the strong dependence of the tensile strength on the fiber volume fraction required further investigation, since, under ideal conditions, one would not expect the normalized tensile strength to vary with fiber fraction.

The highest normalized tensile strength recorded was 75%, lower than the theoretical value of 100%. Composite porosity, fiber misalignment, poor interfacial bonding, a nonuniform distribution of fibers in the matrix, and poor matrix properties all can cause low composite tensile strengths. As mentioned earlier, most of the composites contained less than 5% voids. Gunyaer [24] tested epoxy/carbon composites, which contained 7% and 0.8% voids, and reported that void fraction had a negligible influence on tensile strength. Therefore, the void fractions of the composites tested in the present study do not explain the low tensile strengths. Fiber misalignment can diminish the tensile strength tremendously, but one would expect the misalignment of fibers in the present study to be less than 5°. This is estimated from the length of the frame and the distance between the prepreg guides, and the mold lay-up procedure employed in the study.

The tensile moduli were determined with the aid of strain gages. Figure 29 shows the tensile moduli for all samples as a function of fiber volume fraction. The line represents the theoretical tensile modulus, E_{th}, which is given by the rule of mixtures as:

$$E_{th} = E_m (1-x_{fv}) + E_f (x_{fv}) , \qquad (25)$$

where E_m = 4.8 GPa [21], modulus of LaRC-TPI,

E_f = 231 GPa [14], modulus of the T 300 fibers,

x_{fv} = fiber fraction.

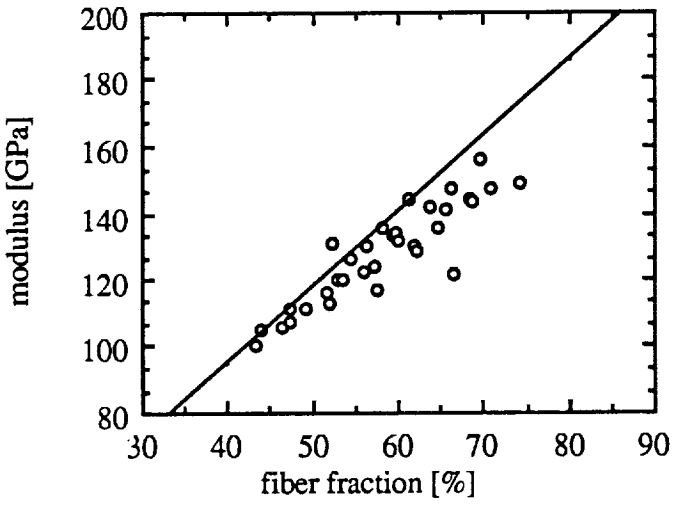

Figure 29. Tensile modulus of all composites.

While the measured moduli of composites with fiber fractions up to 50% corresponded with the moduli given by equation 25, the moduli of composites with high fiber fractions were smaller than expected. This implies that a portion of fibers in the composites with high fiber volume fraction were not loaded completely due to poor load transfer between fibers. This probably led to a nonuniform distribution of stress along the cross section, which caused stress peaks in the composite and therefore, premature failure. Also, this explained the low tensile strength values of composites with high fiber fraction. Diminished load transfer can be attributed to a poor interfacial bonding or to poor matrix properties. Therefore, the dynamic mechanical test and the short beam shear test were conducted to achieve information about the interfacial bonding.

4.3.2 Short Beam Shear Test

Short beam shear testing was conducted on 10 test specimens made from prepreg A and 10 specimens made from prepreg B. The consolidation parameters for all samples were similar (45 min cure time with vacuum). Table 4 shows the shear strengths of the specimens (only the specimens which failed in a true shear mode are reported). As the table shows, the average shear strengths of both groups of specimens were equal. This result indicates that the two different heating systems used on the coating line do not influence the shear properties of the composites. Also, these results show that the shear strength and, thus, the interface between fiber and matrix is adequate. Banerjee [19] measured a shear strength of 73.4 MPa for epoxy/T 650 composites with a fiber volume fraction of 42%. Even though the resin-fiber system used in the present study differs significantly from Banerjee's, the higher shear strength values for LaRC-TPI/T 300 composites tested in the present study is indicative of good fiber/matrix bonding. Thus, poor interfacial bonding of the composites does not explain the low tensile strength values reported in section 3.3.1.

Table 4. Results of Short Beam Shear Test.

	Prepreg A (Electrical Rollers)	Prepreg B (Two Convection Ovens)
Shear strength [MPa]	118.8±3.5	120.0±3.7

± denotes standard deviation.

4.3.3 Dynamic Mechanical Characterization

In addition to the short beam shear test, dynamic mechanical testing was utilized to characterize the interfacial bonding. Three 22.9 cm long bars from each of the four groups (prepreg A with 30 min cure time, with 45 min cure time, with 45 min cure time and vacuum, and prepreg B with 45 min and vacuum) were cut into three 64 mm long specimens. These specimens were subjected to dynamic mechanical tests at room temperature. The Rheometrics RDS 7700 spectrometer applied a maximum strain of 0.1%. All specimens were tested over a range of 0.1 rad/s to 25 rad/s. Each individual specimen was tested twice and, thus, a total of six runs were performed on each of the 12 samples. The dynamic mechanical testing yielded the storage modulus, G', the loss modulus, G", and the tan δ for each specimen.

The dynamic properties of the samples made from prepreg B were plotted versus frequency (Figures 30, 31 and 32). Each data point on these figures represents the average value obtained for six tests. Figure 30 shows that the storage modulus, G', increased with increasing fiber volume fraction. Since the storage modulus of a composite is mainly influenced by the stiff fibers, which are essentially elastic in nature, one would expect an increasing of G' with increasing fiber fraction and an invariance of G' with frequency. The loss modulus, G", increased with increasing fiber fraction as well. This is expected also, since the interfacial area is proportional to fiber volume fraction. The increased interfacial area has been shown to introduce more viscous effects, thus increasing G" [23]. Since both, G" and G' increased with increasing fiber fraction, tan δ, the ratio of G" and G', was found to be less sensitive to the fiber fraction. The loss modulus, G", and tan δ decreased with increasing frequency because they represent the viscous element in the composites. The dynamic response of all other samples was similar to that described above.

The dynamic properties of all composites at a frequency of 0.1585 s^{-1} are shown in Figures 33, 34, and 35. Disregarding the small amount of scatter the figures indicate that all composites had similar dynamic mechanical properties for a given fiber volume fraction.

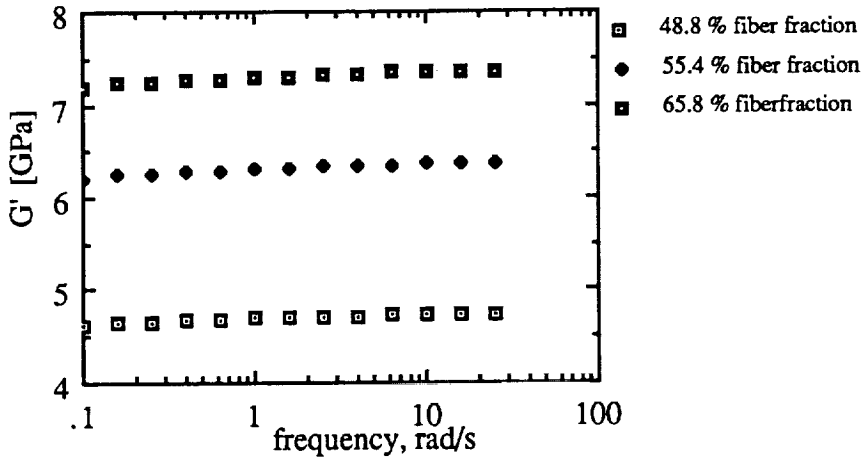

Figure 30. Storage modulus of composites made from prepreg B.

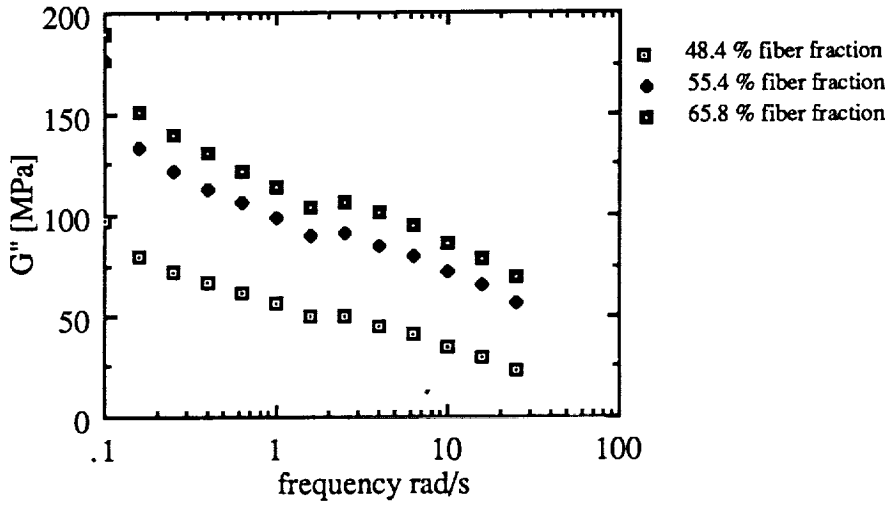

Figure 31. Loss modulus of composites made from prepreg B.

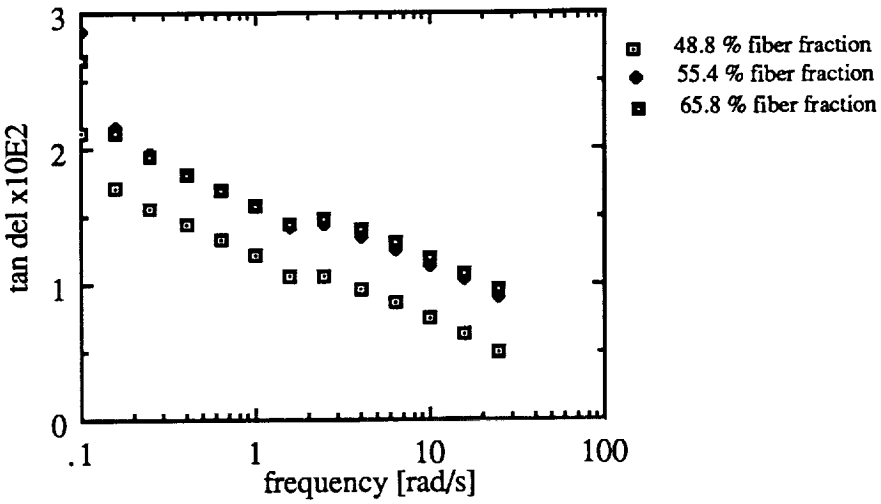

Figure 32. Tan δ of composites made from prepreg B.

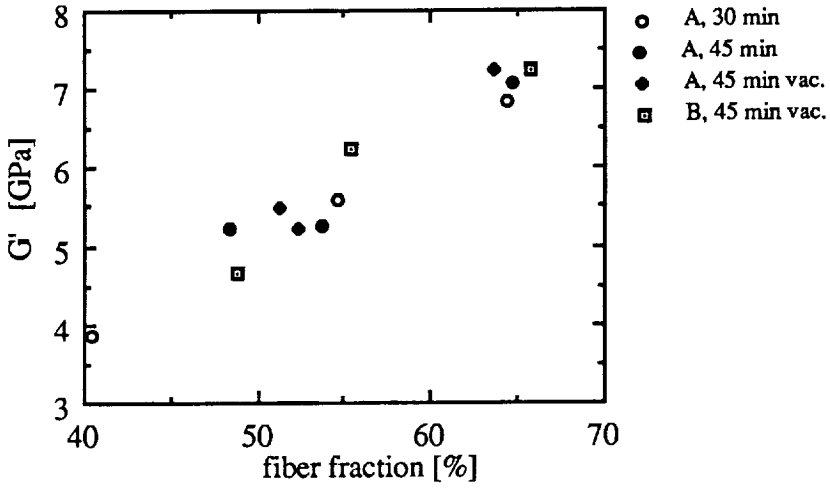

Figure 33. Storage modulus of composites at 0.1585 s^{-1}.

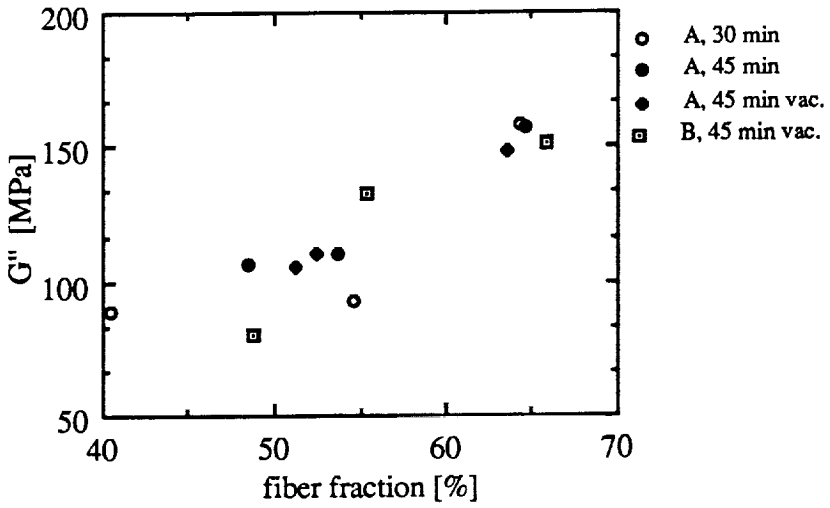

Figure 34. Loss modulus of composites at 0.1585 s^{-1}.

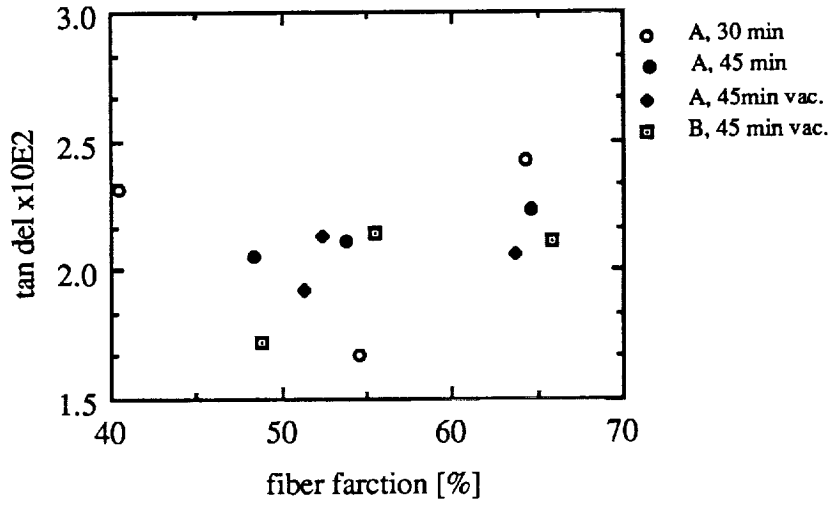

Figure 35. Tan δ of composites at 0.1585 s^{-1}.

Cano [23] determined the dynamic properties of epoxy/AS-4 composites and composites with the same epoxy matrix but formed from pitch-based fibers. For a volume fraction of 60% and a frequency of 0.1585 s^{-1}, Cano [23] reported a tan δ of 1.55×10^{-2} for the epoxy/AS-4 composite, which is slightly lower than the tan δ values in this work. However, composites containing pitch-based fibers had tan δ values of up to 4.53×10^{-2}. The average tan δ obtained in the present study for the LaRC-TPI/T 300 composites was 2×10^{-2}. This value is comparable to that obtained by Cano [23] for AS-4/epoxy composites and considerably below the value obtained for epoxy/pitch-based fiber composites, indicating good interfacial bonding.

Both, the short beam shear test and the dynamic mechanical test showed that the composites made with the coating line had good interfacial bonding. Since fiber misalignment and voids seemed to be unlikely reasons for the low tensile strengths, poor matrix distribution, or the matrix material itself, may have caused this problem. It is possible that the LaRC-TPI powder may create poor matrix properties. The high viscosity of this thermoplastic may prevent the powder particles from forming a coherent tough matrix. Although Gantt [1] and Allen [2] reported good matrix distribution of composites produced from prepreg made on the coating line, matrix distribution problems, inhibiting load transfer between the fibers, can not be discounted in this work. This role of the matrix, the load transfer between the fibers, becomes more important in composites with high fiber volume fraction because the amount of matrix material is reduced. Indeed, while the composites with high fiber volume performed very poorly in tensile testing, lower volume fractions exhibited nearly theoretical tensile strengths.

CHAPTER 5

CONCLUSIONS

The following conclusions may be drawn from the results of the investigation:

1. Most of the composites tested had a void content of less than 2.5%. These low void contents were the direct result of rapid heating of the powder coated prepreg during consolidation. Moisture and other volatiles in the LaRC-TPI powder were found to increase the void fraction.

2. Neither an extension of the cure time nor vacuum reduced the void fractions significantly below those of composites cured for 30 minutes.

3. The use of different types of heating sections did not influence the mechanical properties of the final composites. Interfacial bonding between matrix and carbon fibers, and composite tensile strength were found to be insensitive to the variation of cure time and vacuum during composite fabrication.

4. The results of both the dynamic mechanical analysis and short beam shear testing indicate that the interfacial bonding in composites formed from LaRC-TPI/carbon towpreg is adequate.

5. The moderate tensile strength of the composite specimens is most likely caused by either the matrix material itself or by uneven distribution of the matrix material.

APPENDICES

Appendix A

Wheatstone Bridge

In order to accurately determine the tensile modulus of the specimen, both the load and the strain must be measured precisely during testing. The load cell indicates the total tensile load which is carried by the specimen. Strain gages can be used to evaluate the strain. The strain gage adhered to the specimen operates on the principle that the electrical resistance of the gages varies with the applied strain. The dimensionless relationship between the change in length, ΔL, and the change in gage resistance, ΔR, is defined as gage factor k:

$$k = \frac{\Delta R/R}{\Delta L/L} \quad , \tag{A1}$$

where R = initial resistance of the gage,

L = initial length of the gage,

ΔL = change of the length of the gage,

ΔR = change of the resistance of the gage.

The gage factor depends on the strain gage conductor and lies in the range from 2 to 2.2 for the widely used material Constantan [25]. Since the strain of carbon fiber reinforced composites in the fiber alignment direction is two percent or less, the change in resistance is very small. The Wheatstone bridge can detect such minute differences with sufficient precision to accurately determine the composite strain.

The bridge can consist of one to four active strain gages connected in a specific pattern, across which an excitation voltage is supplied. Such bridge is shown in Figure A1. The relationship between the excitation voltage and the output voltage are related by the resistances:

$$\frac{V_{out}}{V_{exci}} = \frac{R_1 R_3 - R_2 R_4}{(R_2 + R_3)(R_1 + R_4)} \quad , \tag{A2}$$

with V_{out} = output voltage,

V_{exci} = excitation voltage,

R_1 to R_4 = resistances.

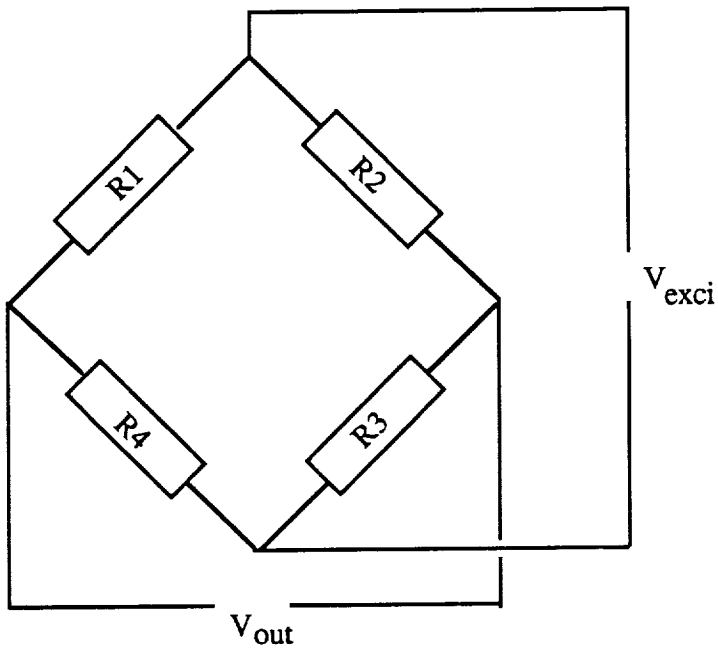

Figure A1. Wheatstone bridge.

Assuming that all resistors and strain gages employed in the Wheatstone bridge have the same resistance, the output voltage equals zero. If the resistance of a strain gage is changed by applying a strain, the output voltage will differ from zero. In order to cancel a bending strain, which can occur during tensile testing, two strain gages are attached parallel to the stress orientation on opposite sides of the specimen. These gages must also be positioned in two opposite legs of the bridge. In this manner, pure bending of the composite will induce a positive strain in one strain gage and a negative strain in the other. For example, if bending is applied causing a 2% change in the resistance of each gage, assuming that the initial resistances of all components are the same, then the output voltage is negligible:

$$\frac{V_{out}}{V_{exci}} = \frac{(R+\Delta R)(R-\Delta R) - R^2}{(R+R+\Delta R)(R+R-\Delta R)} \quad . \tag{A3}$$

Substituting $\Delta R = R\ 0.02$, this reduces to

$$\frac{V_{out}}{V_{exci}} = \frac{(1.02)(0.98) - 1}{(2.02)(1.98)} = -0.0001 \quad . \tag{A4}$$

The final output of the Wheatstone bridge is an electrical signal, whose magnitude depends on the strain to which the gages are subjected. The output of the bridge causes a indefinite deflection of the readout instrument pen. Therefore, a calibration is necessary to calculate the strain associated with the signal from the bridge. This electrical calibration is relatively easy. First, an additional resistor, shunted parallel to a non-strain gage resistor, generates a definite bridge imbalance. This bridge imbalance can be looked upon as a synthetic controlled strain and, as such, appears on the connected readout. The closed circuit with the parallel shunted resistor illustrated in Figure A2. Applying equation A2 to this system, assuming that all resistors R_1 to R_4 are equal:

$$\frac{V_{out}}{V_{exci}} = \frac{R^2 - R\,R'}{(R+R)(R+R')} \quad , \tag{A5}$$

with

$$R' = \frac{R_{par}\,R}{R_{par} + R} \tag{A6}$$

and

R' = parallel shunted resistor,

R_{par} = effective resistance of parallel resistor.

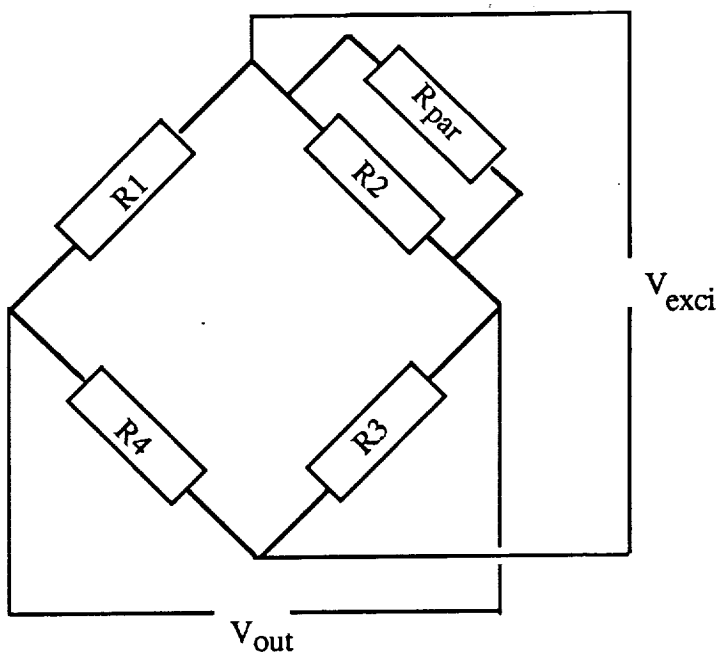

Figure 2. Wheatstone bridge with calibrating resistor.

In the case of two strain gages employed in the bridge at R_1 and R_3, as mentioned previously, the synthetically controlled imbalance equals a fictitious change in resistance in the strain gages, which can be determined by :

$$\frac{V_{out}}{V_{exci}} = \frac{R^2 - R\,(R')}{(R+R)\,(R+R')} = \frac{(R+\Delta R)\,(R+\Delta R) - R^2}{(R+R+\Delta R)^2} \quad , \qquad \text{(A7)}$$

where ΔR is the change in resistance of a fictitious strain. The value of the fictitious strain can then be calculated from A1.

With the aid of these equations, the parallel resistor simulates a strain which can be used to set the full scale reading of the readout instrument. Consequently, a calibrated indication of the readout corresponds to a calculated strain.

These equations were applied in this work. The maximum strain was chosen as 2%. The Wheatstone bridge, consisting of two constant resistors and two strain gages with

wires, was furnished with a 1434 ohm-resistor shunted parallel to one constant resistor. If all resistors in the bridge had the same resistances, the parallel shunted resistor would simulate a 2% strain. Unfortunately, due to the resistances of the wires used, the resistances in the legs of the bridge were different. Therefore, for every specimen the resistances of both the strain gages and the wires were measured by a voltmeter. Since the measured resistances of the strain gages did not lie in the range (120 ohm ± 0.5%), indicated by the producer and were always less 120 ohms, the voltmeter measurements probably exhibited some small error. However, this error is irrelevant to the calculation performed here, since the assumed error canceled in the equation.

For instance, the following calculation was conducted for specimen 53 (Figure A3):

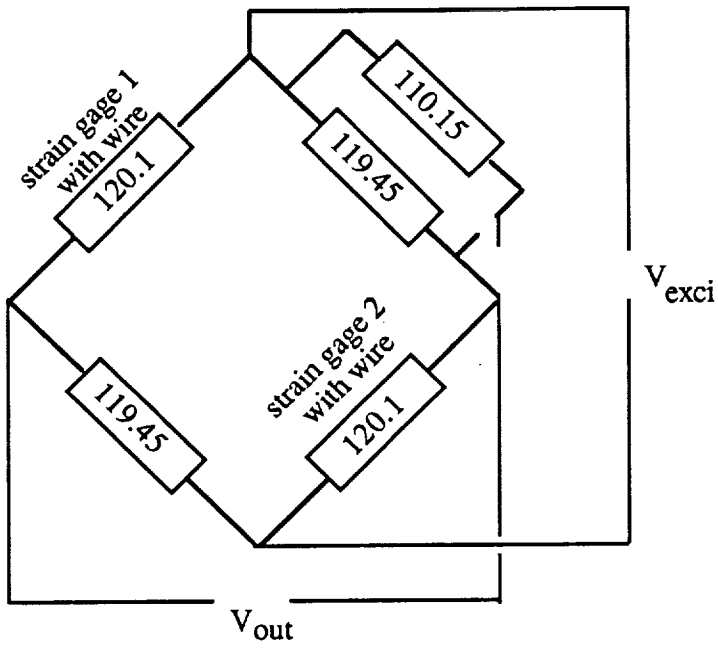

Figure A3. Wheatstone bridge with measured resistances (Sample 53).

First, the different resistances were measured. The voltmeter indicated the following values:

Strain gage 1 with the wire used	=	118.8 ohm + 1.3 ohm = 120.1 ohm,
Strain gage 2 with the wire used	=	118.8 ohm + 1.3 ohm = 120.1 ohm,
R_2	=	119.45 ohm (constant for all samples),
R_4	=	119.45 ohm (constant for all samples),
R_2 with R_{par}	=	110.15 ohm (constant for all samples).

Using the equation A5, the unbalance caused by the parallel-shunted resistor was found:

$$\frac{V_{out}}{V_{exci}} = \frac{120.1^2 - 110.15\ 119.45}{(120.1 + 119.45)\ (120.1 + 110.15)} = 0.0022964 = Y \ . \qquad \text{(A8)}$$

The imbalance, defined as Y, corresponded to the fictitious strain. The strain could be calculated with the aid of equations A7, A2, and using equation A1:

$$\frac{(118.8 + 1.3 + 118.8\ k\ \varepsilon)^2 - 119.45^2}{(118.8 + 1.3 + 119.45 + 118.8\ k\ \varepsilon)^2} = Y \ . \qquad \text{(A9)}$$

Equation A9 is a quadratic equation. Its solution leads to

$$k\ \varepsilon = 0.04179\ , \qquad \text{(A10)}$$

with k = 2.05 (gage factor). The strain, ε, was calculated to be

$$\varepsilon = 2.039\ \%. \qquad \text{(A11)}$$

The Wheatstone bridge now could be calibrated, because the calculated imbalance induced a reproducible deflection on the plotter of the Instron testing machine.

Appendix B

Sample Calculation

Mold Lay Up

In order to determine the number of strips needed to form a composite with the desired thickness, the fiber volume fraction, x_{fv}, of the wound tow must be known. For a cross section of the composite, A, the number of pregregs, N_{req}, is given by

$$N_{req} = \frac{d_f}{d_{ln}} A\, x_{fv} \quad , \tag{B1}$$

where d_f = 1.76 g/cm^3, fiber density [14],

d_{ln} = 3.895 10^{-3} g/cm, linear mass.

The Sample 32 is used to illustrate this calculation. The desired cross section of sample 32 was 1.27 cm by 0.159 cm. Since the desired cross section was the same for almost all composites, and the same tow and polymer was used for all samples, the constant factors could be summarized as follows:

$$N_{req} = \frac{1.76\ g/cm3}{3.895\ 10^{-3}\ g/cm}\ (1.27\ cm)(\ 0.159\ cm)\ x_{fv} = 91.244\ x_{fv} \tag{B2}$$

x_{fv} can expressed by the fiber mass fraction, x_{fm}, with the following equation :

$$x_{fv} = \left(1 + \frac{d_f}{d_p} \left(\frac{1 - x_{fm}}{x_{fm}} \right) \right)^{-1} \quad , \tag{B3}$$

where d_p = 1.4 g/cm^3, density of LaRC-TPI [15].

The fiber mass fraction, x_{fm} was determined with the aid of :

$$x_{fm} = \frac{L\, d_{ln}}{G} \quad , \tag{B4}$$

where G = weight of the coated tow wound onto the frame,

L = total length of the prepreg.

The length, L, of the wrapped tow is the sum of all the single strips. As Figure B1 shows, the length of one strip consists of two parts.

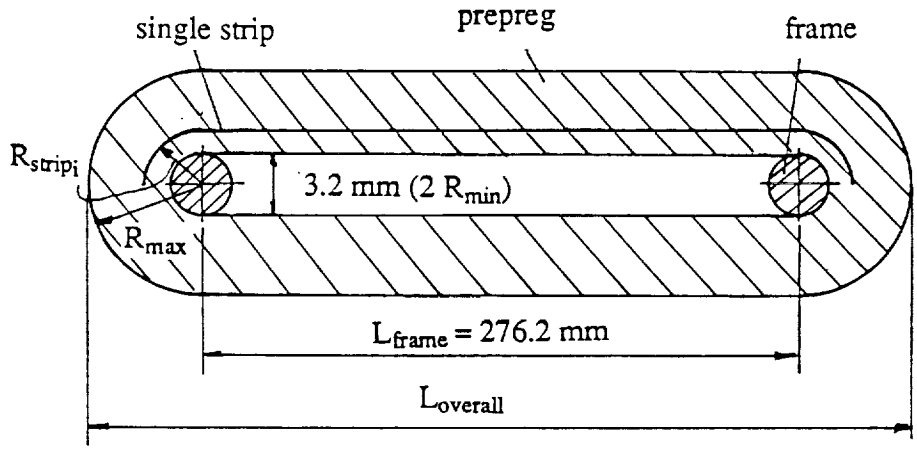

Figure B1. Schematic illustration of the wrapped prepreg.

$$L = \sum_{i=1}^{n} L_{strip_i} = n\, L_{frame} + \pi \sum_{i=1}^{n} R_{strip_i} \quad , \tag{B5}$$

where $$\pi \sum_{i=1}^{n} R_{strip_i} = n\, \pi\, R_{aver} \quad , \tag{B6}$$

and R_{aver} = mean radius of all radii.

The mean radius can be determined using following equation:

$$R_{aver} = \frac{1}{2} (R_{min} + R_{max}) \quad , \tag{B7}$$

where

R_{min} = 0.159 cm, radius of the frame tube,

$$R_{max} = \frac{1}{2} (L_{overall} - L_{frame}) \quad . \tag{B8}$$

The overall length, $L_{overall}$, can be measured with a ruler. The length of the frame, L_{frame}, and R_{min} are known for the wrapping frame used. The required number of strips after the first 30 strips for sample 32 was:

$$R_{max} = 0.5\ (28.6\ \text{cm} - 27.62\ \text{cm}) = 0.49\ \text{cm} \tag{B9}$$

$$R_{aver} = 0.5\ (0.159\ \text{cm} + 0.49\ \text{cm}) = 0.32\ \text{cm} \tag{B10}$$

$$L = 30\ (27.63\ \text{cm} + 3.14 \cdot 0.32\ \text{cm}) = 858\ \text{cm} \tag{B11}$$

The mass for the first 30 strips, G_{30}, was determined using a balance

$$G_{30} = 6.18\ \text{g}. \tag{B12}$$

Equation B4 yielded the fiber mass fraction of the tow, x_{fm}:

$$x_{fm} = \frac{858\ \text{cm}\ 3.895\ 10^{-3}\ \frac{\text{g}}{\text{cm}}}{6.18\ \text{g}} = 0.54\ . \tag{B13}$$

Using Equation B3, it was:

$$x_{fv} = \left(1 + \frac{1.76\ \frac{\text{g}}{\text{cm}^3}}{1.4\ \frac{\text{g}}{\text{cm}^3}} \left(\frac{1 - 0.54}{0.54} \right) \right)^{-1} = 0.48\ . \tag{B14}$$

The required number of prepreg was calculated to be

$$N_{req} = 91.244\ (0.48) = 44\ .$$

Fourteen additional strips were wrapped around the frame, and the same calculation was repeated. This calculation gave $N_{req} = 45$. Thus, one final prepreg strip was added. Finally, the calculation was conducted again. As recommended in the mold-lay-up procedure, the quotient of real to required number of strips ranged between 1.00 and 1.03. It should be noted that, if the fiber mass fraction of the coated tow is not constant, the determination of N_{req} is an iterative calculation.

Tensile Modulus

The Figure B2 shows the plot obtained from testing a composite using the Instron Tensile Testing Machine. The plotter drew the load and the strain versus time during testing. The full scale of load and strain was calibrated before testing. Since carbon fiber

composites can be considered perfectly elastic, the modulus, E, is a constant and can be determined from the slopes of the stress and strain as illustrated in Figure B2.

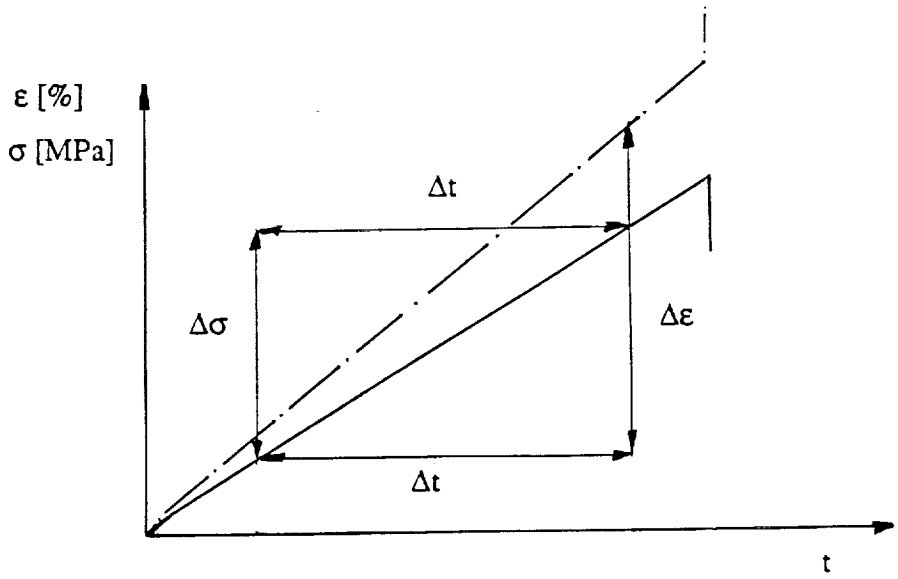

Figure B2. Typical tensile test plot.

$$E = \frac{\Delta\sigma/\Delta t}{\Delta\varepsilon/\Delta t} \tag{B15}$$

Evaluation of Sample 32 provided the following data:

$\Delta\sigma$ = 19.39% of full scale tensile strength (2473 MPa),

$\Delta\varepsilon$ = 20.28% of full scale strain (2.044 %),

Δt = 9 cm (v_{chs}), where v_{chs} is chart speed of plotter.

Finally, $$E = \frac{(0.1939)\ 2473}{(0.2028)\ 0.02044}\ \text{MPa} = 116\ \text{GPa} \tag{B16}$$

Appendix C

Experimental Data

Table C 1. Tensile test properties of composites, cure time 30 minutes, electrical rollers.

Sample	Fiber Fraction [%]	Void Fraction [%]	Tensile Strength [MPa]	Tensile Modulus [GPa]
11	62.0	12.0	852	130
12	59.6	1.7	987	134
13	57.4	15.5	735	117
14	70.7	4.5	784	147
16	54.3	2.2	1061	127
17	66.1	1.7	802	147
20	63.8	9.2	1185	142
31	49.3	2.3	1056	111
32	51.7	2.3	1138	116

Table C 2. Tensile test properties of composites, cure time 45 minutes, electrical rollers.

Sample	Fiber Fraction [%]	Void Fraction [%]	Tensile Strength [MPa]	Tensile Modulus [GPa]
21	65.7	2.0	864	141
22	57.9	4.8	1031	113
23	74.3	13.3	606	149
24	63.4	14.7	End tab failed.	
26	57.3	2.5	End tab failed.	
28	57.1	2.5	1113	124
30	46.5	3.0	1141	106
34	68.5	2.4	519	144
37	40.5	3.1	1063	144

Table C 3. Tensile test properties of composites, cure time 45 minutes, electrical rollers, vacuum.

Sample	Fiber Fraction [%]	Void Fraction [%]	Tensile Strength [MPa]	Tensile Modulus [GPa]
39	53.8	3.9	End tab failed.	
40	43.8	7.7	891	105
43	62.1	3.6	536	129
44	68.7	7.0	601	143
52	53.0	2.6	1207	120
53	55.9	2.2	1204	122
55	55.6	2.0	1281	131
56	53.6	2.0	1138	120
57	64.5	6.1	1018	136

Table C 4. Tensile test properties of composites, cure time 45 minutes, two convection ovens.

Sample	Fiber Fraction [%]	Void Fraction [%]	Tensile Strength [MPa]	Tensile Modulus [GPa]
63	47.2	1.8	1295	107
66	47.4	1.0	1029	111
68	43.4	1.7	988	100
79	56.4	0.5	1116	130
80	66.4	2.7	897	122
81	59.4	0.5	1053	133
82	69.6	4.2	975	156
84	60.1	1.3	1116	131
85	58.2	2.4	1276	135

Table C 5. Short beam shear strengths.

Sample 77 Electrical Rollers Fiber Fraction: 58.4% Void Fraction: 0.2 % [MPa]	Sample 78 Two Convection Ovens Fiber Fraction: 60.9 % Void Fraction: 1.8 % [MPa]
118.8 *	121.3
119.9 *	124.6
119.8 *	123.4
123.1 *	122.3 *
122.0	124.4
122.0	121.2 *
114.4 *	125.6 *
111.7 *	117.5 *
118.8 *	117.4 *
118.4 *	115.8 *
118.1±3.5	120.0±3.7

± indicates standard deviation.

* indicates true shear strength failure.

Table C 6. Averaged dynamic properties of Sample 15.

Heating Section: Electrical Rollers
Cure Time: 30 min
Fiber Fraction: 54.6 %. Void Fraction: 1.8 %.

Frequency, rad/s	tanδ x 10^2	G', GPa	G", MPa
0.1000	2.03±.28	5.56±.39	112.0±14.1
0.1585	1.67±.33	5.58±.40	92.4±15.6
0.2512	1.50±.29	5.60±.40	83.5±14.3
0.3981	1.38±.28	5.61±.40	76.9±14.7
0.6310	1.25±.26	5.62±.40	70.1±13.8
1.000	1.16±.26	5.63±.41	64.7±13.7
1.585	1.02±.25	5.64±.41	57.0±13.8
2.512	1.04±.24	5.65±.41	58.3±13.6
3.981	0.94±.24	5.65±.41	52.8±13.7
6.310	0.86±.23	5.66±.41	48.3±12.9
10.00	0.74±.24	5.67±.41	41.7±12.4
15.85	0.64±.25	5.67±.41	35.9±14.0
25.00	0.52±.25	5.63±.41	29.1±14.1

± indicates standard deviation.

Table C 7. Averaged dynamic properties of Sample 19.

Heating Section: Electrical Rollers
Cure Time: 30 min
Fiber Fraction: 64.3 %. Void Fraction: 1.7 %.

Frequency, rad/s	tanδ x 10^2	G', GPa	G", MPa
0.1000	2.92±.92	6.86±.31	198.8±56.4
0.1585	2.43±.78	6.90±.30	166.6±47.9
0.2512	2.15±.73	6.93±.30	147.8±45.3
0.3981	2.03±.73	6.95±.30	139.4±45.6
0.6310	1.87±.71	6.96±.30	129.2±44.9
1.000	1.78±.71	6.98±.30	122.9±45.0
1.585	1.62±.70	6.99±.30	112.0±44.8
2.512	1.64±.70	7.00±.30	113.5±44.4
3.981	1.56±.70	7.02±.30	108.3±45.0
6.310	1.46±.70	7.01±.28	101.3±45.4
10.00	1.37±.71	7.04±.30	95.2±46.0
15.85	1.25±.70	7.05±.30	87.1±45.8
25.00	1.11±.70	7.06±.30	77.5±46.1

± indicates standard deviation.

Table C 8. Averaged dynamic properties of Sample 27.

Heating Section: Electrical Rollers
Cure Time: 45 min
Fiber Fraction: 53.7 %. Void Fraction: 2.5 %.

Frequency, rad/s	tanδ x 10^2	G', GPa	G", MPa
0.1000	2.66±.33	5.23±.38	138.2±10.1
0.1585	2.11±.28	5.26±.39	110.4±9.0
0.2512	1.94±.26	5.28±.39	101.9±8.7
0.3981	1.80±.26	5.29±.39	94.6±9.3
0.631	1.69±.25	5.30±.40	88.9±9.2
1.000	1.57±.24	5.31±.40	82.9±9.5
1.585	1.42±.24	5.33±.40	75.3±9.8
2.512	1.43±.23	5.34±.40	76.1±9.9
3.981	1.34±.22	5.35±.41	71.4±9.7
6.310	1.24±.21	5.35±.41	66.1±9.2
10.00	1.13±.21	5.36±.41	60.2±9.5
15.85	1.02±.22	5.37±.41	54.1±10.5
25.00	0.89±.21	5.37±.41	47.2±9.9

± indicates standard deviation.

Table C 9. Averaged dynamic properties of Sample 29.

Heating Section: Electrical Rollers
Cure Time: 45 min
Fiber Fraction: 48.4 %. Void Fraction: 2.3 %.

Frequency, rad/s	tanδ x 10^2	G', GPa	G", MPa
0.1000	2.59±.90	5.18±.21	134.1±42.7
0.1585	2.04±.65	5.21±.21	106.2±30.6
0.2512	1.84±.60	5.23±.22	96.2±28.7
0.3981	1.72±.57	5.25±.22	90.4±27.5
0.6310	1.62±.56	5.26±.22	85.1±27.0
1.000	1.50±.55	5.27±.22	79.0±26.4
1.585	1.34±.54	5.28±.22	70.6±26.4
2.512	1.37±.53	5.29±.22	72.7±25.8
3.981	1.27±.53	5.30±.22	67.2±26.1
6.310	1.18±.53	5.31±.22	62.8±25.8
10.00	1.08±.52	5.32±.22	57.6±25.7
15.85	0.98±.51	5.33±.22	52.0±25.3
25.00	0.86±.50	5.33±.22	45.8±25.3

± indicates standard deviation.

Table C 10. Averaged dynamic properties of Sample 33.

Heating Section: Electrical Rollers
Cure Time: 45 min
Fiber Fraction: 64.7 %. Void Fraction: 3.6 %.

Frequency, rad/s	tanδ x 10^2	G', GPa	G", MPa
0.1000	2.67±.37	7.05±.57	187.2±20.6
0.1585	2.23±.36	7.09±.58	157.3±20.8
0.2512	2.02±.37	7.11±.58	142.5±22.0
0.3981	1.91±.37	7.12±.58	135.0±22.0
0.6310	1.77±.37	7.14±.58	125.4±22.8
1.000	1.67±.37	7.15±.59	118.3±22.7
1.585	1.53±.37	7.16±.59	108.5±23.2
2.512	1.55±.37	7.71±.59	110.4±23.1
3.981	1.46±.36	7.18±.59	103.9±22.8
6.310	1.36±.36	7.19±.59	97.1±22.6
10.00	1.26±.36	7.20±.59	89.8±22.7
15.85	1.14±.24	7.21±.59	81.7±22.0
25.00	1.03±.33	7.21±.59	73.7±21.4

± indicates standard deviation.

Table C 11. Averaged dynamic properties of Sample 35.

Heating Section: Electrical Rollers
Cure Time: 30 min
Fiber Fraction: 40.5 %. Void Fraction: 3.1 %.

Frequency, rad/s	tanδ x 10^2	G', GPa	G", MPa
0.1000	2.79±.76	3.84±.17	106.5±26.4
0.1585	2.32±.66	3.87±.16	89.3±24.1
0.2512	2.17±.66	3.88±.16	83.9±23.5
0.3985	2.03±.63	3.89±.16	78.6±23.5
0.6310	1.91±.62	3.90±.16	74.4±23.3
1.000	1.79±.62	3.91±.16	69.7±23.2
1.585	1.64±.61	3.92±.16	63.8±23.0
2.512	1.67±.62	3.93±.16	64.7±23.2
3.985	1.55±.60	3.94±.16	60.6±22.9
6.310	1.49±.60	3.94±.16	56.8±22.7
10.00	1.34±.61	3.95±.16	52.5±23.1
15.85	1.21±.61	3.95±.16	47.5±23.1
25.00	1.07±.61	3.96±.16	42.0±23.2

± indicates standard deviation.

Table C 12. Averaged dynamic properties of Sample 51.

Heating Section: Electrical Rollers
Cure Time: 45 min. Vacuum.
Fiber Fraction: 51.2 %. Void Fraction: 1.9 %.

Frequency, rad/s	tanδ x 10^2	G', GPa	G", MPa
0.1000	2.41±042	5.45±.15	131.6±24.0
0.1585	1.92±.28	5.49±.16	105.6±16.1
0.2512	1.77±.25	5.51±.16	97.3±14.4
0.3985	1.63±.23	5.52±.16	90.2±13.2
0.6310	1.54±.21	5.54±.17	85.1±12.4
1.000	1.47±.22	5.38±.49	78.7±11.9
1.585	1.27±.20	5.56±.17	70.7±11.5
2.512	1.30±.20	5.58±.17	72.7±11.6
3.985	1.20±.19	5.59±.17	67.2±11.2
6.310	1.12±.19	5.60±.17	62.9±11.3
10.00	1.02±.18	5.60±.17	57.2±10.8
15.85	0.91±.19	5.59±.17	51.1±11.1
25.00	0.80±.19	5.60±.17	44.8±.10.8

± indicates standard deviation.

Table C 13. Averaged dynamic properties of Sample 54.

Heating Section: Electrical Rollers
Cure Time: 45 min. Vacuum.
Fiber Fraction: 52.4 %. Void Fraction: 2.1%.

Frequency, rad/s	tanδ x 10^2	G', GPa	G", MPa
0.1000	2.44±.46	5.17±.52	125.0±19.8
0.1585	1.93±.26	5.19±.52	99.7±12.2
0.2512	1.72±.20	5.21±.52	89.6±13.0
0.3985	1.61±.20	5.22±.52	83.5±10.6
0.6310	1.48±.17	5.23±.53	77.0±10.6
1.000	1.38±.18	5.24±.53	71.9±10.2
1.585	1.22±.17	5.25±.53	64.1±9.5
2.512	1.24±.18	5.26±.53	64.9±10.2
3.985	1.12±.22	5.44±.79	60.2±10.4
6.310	1.05±.19	5.28±.54	55.0±10.6
10.00	0.92±.18	5.28±.54	48.7±10.5
15.85	0.80±.18	5.29±.54	42.6±10.6
25.00	0.66±.17	5.29±.54	35.1±10.3

± indicates standard deviation.

Table C 14. Averaged dynamic properties of Sample 58.

Heating Section: Electrical Rollers
Cure Time: 45 min . Vacuum.
Fiber Fraction: 63.6 %. Void Fraction: 3.0 %.

Frequency, rad/s	tanδ x 10^2	G', GPa	G", MPa
0.1000	2.58±.56	7.19±.28	184.6±35.4
0.1585	2.04±.44	7.24±.28	146.7±28.1
0.2512	1.89±.35	7.26±.27	136.5±22.5
0.3985	1.74±.32	7.28±.28	126.1±20.5
0.6310	1.62±.28	7.30±.27	118.2±18.0
1.000	1.52±.27	7.31±.28	110.5±17.6
1.585	1.37±.26	7.33+.28	100.2±16.7
2.512	1.39±.25	7.34±.28	102.1±16.2
3.985	1.30±.25	7.36±.28	95.5±16.5
6.310	1.22±.24	7.37±.28	89.3±16.0
10.00	1.12±.22	7.38±.28	82.3±15.0
15.85	1.01±.22	7.39±.28	74.1±14.9
25.00	0.89±.20	7.39±.28	65.2±14.2

± indicates standard deviation.

Table C 15. Averaged dynamic properties of Sample 64.

Heating Section: Two Convection Ovens
Cure Time: 45 min . Vacuum.
Fiber Fraction: 48.8 %. Void Fraction: 1.8 %.

Frequency, rad/s	tanδ x 10^2	G', GPa	G", MPa
0.1000	2.12±.59	4.62±.14	97.9±27.2
0.1585	1.72±.46	4.64±.15	79.8±20.6
0.2512	1.56±.42	4.64±.15	72.4±19.1
0.3985	1.44±.42	4.67±.15	67.0±19.1
0.6310	1.32±.41	4.68±.15	61.6±18.5
1.000	1.21±.40	4.69±.15	56.5±18.4
1.585	1.05±.40	4.70±.15	49.4±18.2
2.512	1.07±.41	4.71±.15	50.0±18.6
3.985	0.96±.40	7.42±.15	45.3±18.1
6.310	0.86±.39	4.72±.15	40.6±18.1
10.00	0.75±.39	4.73±.15	35.2±18.1
15.85	0.63±.39	4.73±.15	29.7±18.0
25.00	0.49±.40	4.74±.15	23.5±18.4

± indicates standard deviation.

Table C 16. Averaged dynamic properties of Sample 67.

Heating Section: Two Convection Ovens
Cure Time: 45 min . Vacuum.
Fiber Fraction: 55.4 %. Void Fraction: 0.7 %.

Frequency, rad/s	tanδ x 10^2	G', GPa	G", MPa
0.1000	2.86±.53	6.20±.36	176.6±29.7
0.1585	2.15±.41	6.24±.37	133.1±19.4
0.2512	1.97±.34	6.26±.37	122.2±16.2
0.3985	1.81±.37	6.27±.37	112.8±15.9
0.6310	1.70±.32	6.29±.37	106.0±15.0
1.000	1.57±.29	6.30±.38	98.5±14.2
1.585	1.43±.28	6.31±.38	89.4±13.8
2.512	1.44±.26	6.32±.38	90.4±12.6
3.985	1.35±.25	6.34±.38	85.0±12.3
6.310	1.26±.25	6.34±.38	79.2±12.4
10.00	1.14±.28	6.35±.39	71.8±12.4
15.85	1.04±.25	6.36±.39	65.4±13.0
25.00	0.90±.24	6.37±.39	56.9±13.0

± indicates standard deviation.

Table C 17. Averaged dynamic properties of Sample 83.

Heating Section: Two Convection Ovens
Cure Time: 45 min . Vacuum.
Fiber Fraction: 65.8 %. Void Fraction: 2.4 %.

Frequency, rad/s	tanδ x 10^2	G', GPa	G", MPa
0.1000	2.66±.70	7.19±.53	189.3±44.1
0.1585	2.12±.50	7.23±.53	151.8±32.3
0.2512	1.94±.50	7.25±.53	139.2±32.3
0.3985	1.81±.48	7.27±.53	130.4±32.3
0.6310	1.69±.49	7.28±.53	121.8±33.5
1.000	1.58±.47	7.29±.53	114.2±32.7
1.585	1.44±.48	7.31±.54	104.3±33.7
2.512	1.40±.48	7.32±.54	107.0±33.8
3.985	1.40±.47	7.33±.54	101.5±33.7
6.310	1.30±.48	7.34±.54	94.7±34.2
10.00	1.19±.46	7.35±.54	86.5±33.6
15.85	1.08±.44	7.36±.55	78.7±32.4
25.00	0.96±.43	7.37±.55	67.9±32.0

± indicates standard deviation.

Appendix D

Materials

Carbon fiber. Thornel T-300 6K, unsized, manufactured by Amoco Performance Products, Inc., Greenville, SC. Used in all prepregs.

Polyimide powder. LaRC-TPI #1500, lot # 24-703, manufactured by Mitsui Toatsu Chemicals, Inc., Tokyo, Japan.

Mold release. Frekote FRP aerosol, 400 ml, manufactured by Hysol Div. of the Dexter Corp., Seabrook. Used on composite mold surfaces to avoid sticking.

Bagging foil. Thermalide - 002, 60" wide roll, manufactured by Airtech Intl., Inc., Carson, CA. Used to bag composite mold during specimen formation.

Vacuum bag sealing tape. A 800 3 G, manufactured by Airtech Intl., Inc., Carson, CA. Used to seal vacuum bag.

End tab adhesive. Scotch Weld Brand EC 3569 B/A, epoxy based two-part adhesive, manufactured by Adhesives, Coatings and Sealers Division / 3M, St. Paul, MN. Used to bond the aluminum end tabs to the tensile test specimen.

Strain gages and allied accessories. Strain gage CEA-06-240UZ-120, gage factor 2.05. M-Bond 200 Adhesive, 200 Catalyst, M-Prep Neutralizer 5A, M-Prep Conditioner A, manufactured by Micromeasurements Inc., Romulus, MI. Used to record the strain during tensile testing.

Appendix E

Equipment

Coating line. Designed by Laurence E. Allen [2] and B. Gantt [1]. Improved spreader and deposition chamber by James Klett [13]. Used to produce the carbon fiber prepregs.

Composite mold. Custom design. Fabricated by Clemson University Engineering Services. Used to making the composite sample bars.

High temperature press. Carver Laboratory Press Model #2529, manufactured by Fred S. Carver inc., Menomone, WI. Used to apply heat and pressure when making composites.

Mold top lifter. Custom design. Fabricated by Department of Chemical Engineering Workshop. Used to lift the top part of the mold following composite formation.

Short beam shear test fixture. Custom design. Fabricated by Clemson University Engineering Services. Design based on fixtures used by Banerjee [19] and Diwan [22]. Used to conduct the short beam shear test.

Instron universal testing machine. Model 1125, manufactured by Instron Corp. Used to carry out the tensile tests and the short beam shear tests.

Rheometrics dynamic spectrometer. Model 7700, manufactured by Rheometrics, Inc., Pascataway, NJ. Used to conduct dynamic mechanical tests. This machine was equipped with an IBM PS/2 computer.

Wheatstone bridge. Custom design. Fabricated by the author. Used to interface strain gages and strain data recorder of the Instron 1125 machine.

LITERATURE CITED

1. Gantt, B. W., M.S. Thesis, Clemson University, Clemson SC, (May,1987).

2. Allen, L. E., M.S. Thesis, Clemson University, Clemson SC, (August, 1989).

3. Mallick, P.K., "Fiber-reinforced Composites: Materials, Manufacturing, and Design," Marcel Dekker, Inc., New York, NY (1988).

4. Robbins, D., "Carbon Fibres Composites in General Engineering Practice," Fothergill & Harvey Ltd.

5. Wolff, E. G., "Dimensional Stability of Structural Composites for Spacecraft Application," Metal Prog,115:54 (1979).

6. Fitzer, E., "Carbon Fibres and Their Composites," Springer Verlag, New York, NY, 1985.

7. English, L. K., "Fabrication the Future with Composite Materials; Part 3," ME, 33-37 February,1987.

8. Michaeli, W., "Faserverbundwerkstoffe," RWTH Aachen, Wintersemester 1989/90.

9. Johnston, N.J., P. M. Hergenrother, "High Performance Thermoplastics: A Review of Neat Resin Properties," 32nd Intl. SAMPE Symp., April 6-9 (1987).

10. Quinn, K. R., G. O'Brien, "Thermoplastic Composites for the Hot Jobs," Machine Design, February 11 (1988).

11. Burks, H. D., T. L. St. Clair, and T. H. Hou, "Characterization of Crystalline LaRC-TPI Powder," SAMPE Quart., (18) 1, 1-8 (1986).

12. Baucom, R. M., J. M. Marchello, "LaRC Dry Powder Towpreg System," NASA Technical Memorandum 102648, April (1990).

13. Klett, J., Research for M.S. Thesis, Clemson University, Clemson SC, (August, 1991).

14. Product Literature,"Thornel Pan Based Fibers," Amoco Performance Products, Inc., (1989).

15. St. Clair, A. K., T. L. St. Clair, "A Multi Purpose Thermoplastic Polyimide," SAMPE Quart., October (1981).

16. Product Literature, "Student Manual for Strain Gage Technology," Measurement Group, Inc., Education Division, Raleigh, NC 27611 (1983).

17. ASTM-Standard D 3039-76 (1989).

18. ASTM-Standard D 2344-84 (1989).

19. Banerjee, A., Ph.D. Dissertation, Clemson University, Clemson SC, (December, 1989).

20. Baur, W., "The Influence of the Interlaminar Shear Strength of Carbon-Carbon Composites on the Testing of Materials and on the Design of Structural Parts," SIGRI GmbH, Meitingen, FRG.

21. Ohta, W, S. Tamai, T. W. Towell, N. J. Johnston, and T. L. St. Clair, "Improved Melt and Physical Properties of Mistui Toatsu's LaRC-TPI # 1500 Series Polyimide," Mitsui Toatsu Chemicals, Inc., Central Research Laboratory (1990).

22. Diwan, P., M.S. Thesis, Clemson University, Clemson SC, (December, 1985).

23. Cano, R. J., M.S. Thesis, Clemson University, Clemson SC, (August, 1990).

24. Gunyaer, G. M. ,"The Effect of Structure Processing Defects on Mechanical Properties of Polymeric Composites," HANDBOOK OF COMPOSITES, Vol. 3, Elsevier Science Publishers B.V., 1985.

25. Perry, C. C., H. R. Lissner, "The Strain Gage Primer," McGraw-Hill Company, Inc., New York, 1962.